

https://dspace.org/

Kinetics of leaching of a low grade matter in ferric sulphate solution

2015-03-05
http://hdl.handle.net/10539/17196

Downloaded from a DSpace repository. https://dspace.org/

KINETICS OF LEACHING OF A LOW GRADE MATTE IN FERRIC SULPHATE SOLUTION

Michael John Dry

A thesis submitted to the Faculty of Engineering,
University of the Witwatersrand, Johannesburg,
in fulfilment of the requirements for the degree
of Doctor of Philosophy

Johannesburg 1984

DECLARATION

I declare that this thesis is my own, unaided work, except where specific acknowledgement is made. It is being submitted for the degree of Doctor of Philosophy in the University of the Witwatersrand. It has not been submitted before for any degree or examination in any other University.

M.J. DRY

22nd day of May 1984.

ABSTRACT

The leaching of low grade matte in acid ferric sulphate sulphate (100 g/l Fe^{3+}) solution has been studied, and shown to be electrochemical in nature. The matte was quantitatively analysed and found to contain troilite, an iron-nickel alloy, a copper-iron sulphide and magnetite, as separate phases. Based on the matte analysis, a shrinking-particle model, combined with an electrochemical leaching rate expression, successfully predicted the dissolution curves for the nickel, copper, cobalt and iron in the matte, in a batch reactor. The potential of the matte particles during leaching was best approximated by the solution redox potential. The solution redox potential was successfully predicted by the Nernst equation plus Debye-Hückel activity coefficients, when the various ferric and ferrous sulphate complex equilibria were taken into account. The formation of elemental sulphur on the matte particles did not affect the leaching rate.

ACKNOWLEDGEMENTS

Firstly, I wish to thank the Council for Mineral Technology for allowing me to do this work, on full salary, in their laboratories, and for the use of their analytical services. I also thank the Anglo American Corporation for allowing this project to arise out of one of their sponsored projects at the Council for Mineral Technology.

I gratefully acknowledge the interest in, and assistance given to, my project by the following people:

Dr E J Oosthuyzen, Mr E A Viljoen and Mrs J Nostert, for doing the quantitative analysis of the matte. Without this quantitative analysis, this work would have lost much of its significance.

Dr M J Nicol and Dr R L Paul, for several very instructive discussions of the electrochemistry of leaching. The insight gained from these discussions greatly facilitated this work.

Also, I wish to thank my supervisor, Prof A W Bryson, for the excellent guidance given to me throughout the duration of this work, and during the writing of this thesis.

Dr W A M Te Riele and Dr L J Dry made useful suggestions on the writing of this thesis. The time they spent reading parts of the first draft and making these suggestions is gratefully acknowledged.

Last but not least, I wish to express my gratitude to Mrs M W Britz for typing this thesis.

CONTENTS

ABSTRACTS	i
ACKNOWLEDGEMENTS	ii
1. PREFACE	1
1.1 Introduction	1
1.2 Literature survey	2
1.3 Scope of the present study	15
1.4 Criteria for a mathematical model	16
2. EXPERIMENTAL	17
2.1 Description of matte	17
2.1.1 Mineralogy and chemical composition	17
2.1.2 Particle size distribution	23
2.1.3 Physical appearance	25
2.1.4 Degree of liberation	27
2.2 Leaching of matte	28
2.2.1 Leaching apparatus	28
2.2.2 Matte and residue electrodes	30
2.2.3 Leach solution	32
2.2.4 Leaching procedure	32
2.2.5 Sample analysis	33
2.2.6 Calculation of extractions during leaching	33
2.2.7 Leaching conditions	35
2.3 Measurement of solution redox potential	35
2.3.1 Apparatus	35
2.3.2 Procedure	35
2.4 Electrochemical measurement of matte leaching rate as a function of potential	38
2.4.1 Apparatus	38
2.4.2 Procedure	38
3. RESULTS	40
3.1 Leaching of matte	40
3.2 Measurement of solution redox potential	42
3.3 Electrochemical measurement of matte leaching rate as a function of potential	42

3.4 Deportment of sulphur 43
3.5 Effect of temperature on leaching rates 45

4. THEORETICAL MODELLING OF THE EXPERIMENTAL RESULTS 47
4.1 Leaching of matte 47
4.1.1 Derivation of the model 54
4.1.1.1 Mineral surface behaviour 54
4.1.1.2 Effect of the leach solution 59
4.1.1.3 Prediction of the dependence of the leaching rate of FeS on the mineral surface potential 62
4.1.1.4 Prediction of the dependence of the leaching rate of the alloy phase on the mineral surface potential 64
4.2 Solution redox potential 65
4.2.1 The Nernst equation 65
4.2.2 Complex species formed 72
4.2.3 Estimation of stability constants at zero ionic strength 75
4.2.4 Assumption implicit in the use of the Nernst equation 77
4.3 Electrochemical measurement of the matte leaching rate 78

5. APPLICATION OF THE THEORY TO THE EXPERIMENTAL RESULTS 80
5.1 Leaching rate model 80
5.1.1 Effect of different potentials on the fit of the leaching model 81
5.1.2 Comparison between predicted and experimental dependence of the leaching rate on potential 90
5.2 Solution redox potential 92
5.2.1 Redox potential at ambient temperature 92
5.2.2 Redox potential at elevated temperature 97
5.2.3 Discussion 101
5.3 Combination of the leaching model with the calculation of solution redox potential 104
5.4 Effect of temperature 106
5.5 Dependence of the leaching rate on the unleached mineral remaining 109

6. CONCLUSIONS 111

APPENDIX I 112
Results of matte phase calculations

a) X-ray diffraction data 113
b) Microtrac particle size analyses 119
c) Printouts of phase distribution calculations 120

APPENDIX II 124
Results of leaching experiments - Raw data

APPENDIX III 174
Results of potential measuring experiments

a) Raw data 175
b) Printouts of measured vs predicted results 177

APPENDIX IV 199
Results of electrochemical current-potential curve measurement

a) Raw data 200
b) Computer printout 201

APPENDIX V 202

a) Derivation of the activities of the uncomplexed ferrous and ferric ions in the concentrated sulphate solution 203
b) Calculation of zero-ionic strength stability constants for $FeHSO_4^{2+}$, $FeHSO_4^{+}$ and $FeHSO_4SO_4$ 207

APPENDIX VI 210
Constants used in the Debye-Hückel equation

APPENDIX VII 211
Values of limiting ionic conductivity used for calculation of liquid junction potential

APPENDIX VIII 212
Computer programme of the leaching model

APPENDIX IX 226
Leaching model output-graphs and printouts

APPENDIX X 294
Computer programmes

1) For calculation of solution redox potential 295
2) For fitting electrochemical measurements 306
3) For calculation of the matte phase distribution 311

APPENDIX XI 314
Graphs showing the effect of temperature on the leaching rate constants

REFERENCES 319

1. PREFACE

1.1 Introduction

In conventional pyrometallurgical processing (e.g. roasting, smelting, converting) of base metal sulphides, the sulphide sulphur is converted to sulphur dioxide(37). In general, this sulphur dioxide is either released into the atmosphere, or converted into sulphuric acid. Releasing sulphur dioxide into the atmosphere causes air pollution, and the production of sulphuric acid is not always attractive, as the storage and transportation of sulphuric acid can be costly.

An alternative to pyrometallurgical processing of base metal sulphides is hydrometallurgical treatment. Simple non-oxidative dissolution of sulphide in acid would liberate the sulphide sulphur(36) as gaseous hydrogen sulphide, which would probably be no easier to dispose of than sulphur dioxide. Oxidative leaching, on the other hand, yields elemental sulphur(27) or sulphate in solution(26), depending on the severity of the leaching conditions. This would eliminate the problem of disposing of a noxious sulphur gas. Oxidative leaching has another advantage, namely that it can treat iron-bearing sulphides in such a way that the valuable metals (be they zinc, nickel, copper, etc.) are taken into solution, while the iron in the sulphide is rejected from the solution as an iron hydroxide precipitate, for example, goethite(5, 51,52,53). This means that sulphides containing too much iron for economical pyrometallurgical processing can be processed hydrometallurgically, via oxidative leaching.

As reserves of high-grade sulphides are consumed, lower grades (i.e., containing more iron) will have to be processed. The mineralogy of the lower grade ores will determine the degree of liberation of valuable metals from iron possible by ore-dressing techniques such as flotation, etc. These low grade ores will probably have to be processed hydrometallurgically, one possible route being oxidative dissolution in acid. An understanding of the oxidative dissolution of (especially low-grade iron-bearing) sulphides in acid is therefore of obvious importance.

1.2 Literature survey

From the literature, it seems that there is considerable interest in the oxidative leaching of sulphide minerals. A number of oxidative leaching processes have been patented(51, 54, 55). Forward and Warren(56) reviewed the chemistry of the oxidation of sulphides in aqueous solution, and concluded that the factors controlling the rate of sulphide oxidation could be broadly classified into three groups, i.e., mass transport between the bulk of the solution and the solid surface of reactants or products, formation of coatings of insoluble products on the surfaces of the minerals, and control by chemical reaction at the mineral surface or in the solution. Forward and Warren also found that the sulphide sulphur can be oxidised to elemental sulphur or to sulphate in acid oxidative leaching, and that when elemental sulphur is formed during oxidation of a sulphide below 118°C, the sulphur film produced on the sulphide surface is porous and does not inhibit oxidation of the underlying mineral. Between 118°C and 160°C, molten sulphur coats the mineral surface and inhibits further oxidation (56) while above 160°C, the tendency is for the sulphide to oxidise to sulphate. Forward and Warren also reviewed various oxidative leaching systems. Of the acid systems discussed, they considered the most likely to provide economic leach processes to be sulphuric acid and oxygen, possibly combined with ferric sulphate to act as an "oxygen carrier".

Dutrizac(57) reviewed the literature on the role of the ferric ion in oxidative leaching, and summarised the findings of several studies on the kinetics of leaching various sulphides in acidified ferric sulphate and ferric chloride solutions. From this review, it seems that sulphides of the type MS (M = copper, zinc, lead, iron) dissolve in acid ferric solutions according to the following stoichiometry:

$$MS + 2Fe^{3+} \rightarrow M^{2+} + 2Fe^{2+} + S^{o}$$

The rate of dissolution of these "simple" (MS) sulphides seems, in most cases, to be controlled by chemical reaction, rather than diffusion mechanisms, according to Dutrizac's review. Two exceptions to this generalization are sphalerite (ZnS) and galena (PbS). The dissolution of ZnS was reported to be controlled by ferric diffusion in the solution

while the dissolution of PbS was supposed to be limited by the diffusion of ferric ions through a protective sulphur layer. In the case of chalcocite (Cu_2S), the dissolution proceeds via a solid-state transition, i.e.:

$$Cu_2S + 2Fe^{3+} \rightarrow Cu^{2+} + 2Fe^{2+} + CuS$$

This reaction is rapid(57) when compared to the dissolution of the CuS, which proceeds in the same way as the dissolution of "simple" sulphides. It would appear then that if high extractions of copper from Cu_2S are required, the kinetics of dissolution of CuS will determine factors such as the leaching time, etc. required.

The activation energy for galena dissolution was given as "high" in Dutrizac's review. This is not consistent with liquid phase diffusion of ferric ions(45) through a porous sulphur layer formed below 118°C(56). Brodie(1) and Paul, Nicol, Diggle and Saunders(2) studied the dissolution of galena in sulphate solution, and fitted an electrochemical surface reaction mechanism to their experimental results. This would seem to refute the theory in Dutrizac's review of a protective sulphur layer inhibiting the dissolution of galena.

In the study summarised by Dutrizac(57) of ZnS dissolution (in acid ferric sulphate solution), an activation energy of about 25 kJ/mol was measured, which is consistent with control by liquid phase diffusion(45). On the other hand, Rath, Paramguru and Jena(28) studied the dissolution of sphalerite in acid ferric chloride solution and found an activation energy of about 90 kJ/mol, which is too high for control by liquid phase diffusion (which has activation energies of between about 8 and 25 kJ/mol(45). Rath *et al* assumed the rate to be controlled by the inward diffusion of ferric ions through a protective sulphur layer around the sphalerite particles. However, their investigation was done at temperatures between 30°C and 70°C, and Forward and Warren (56) concluded that the sulphur formed on a reacting sulphide surface at temperatures below 118°C is porous, and does not inhibit oxidation of the underlying mineral. If this is so, then the sulphur formed on the ZnS particles during leaching between 30°C and 70°C would be porous, and ferric diffusion would occur in the liquid in the pores. Madsen(45) measured the diffusivity of the ferric ion in concentrated sulphate solution, and found an apparant activation energy for ferric diffusion

of 22,4 kJ/mol, which is considerably lower than the value of the activation energy of 90 kJ/mol reported by Rath *et al*. While the diffusivity of the ferric ion may be expected to differ in solutions of ferric sulphate and ferric chloride, this difference is not likely to be large enough to account for the much higher activation energy for the dissolution of ZnS in acid ferric chloride solution, thus it seems likely that some other mechanism controls the rate of oxidative leaching of sphalerite. Jan(33) studied the kinetics of oxygen pressure leaching of sphalerite in sulphuric acid, and concluded that the rate-determining step is the oxidation of H_2S (formed by direct acid attack on the ZnS), on the mineral surface, by the ferric ion - i.e. chemical reaction control. Verbaan(35) studied the dissolution of sphalerite in sulphuric acid and in acid ferric sulphate solutions. He used Langmuir-Hinshelwood adsorption theories to explain the observed kinetics, but found conflicting evidence as to whether or not the elemental sulphur formed on the sphalerite surface resulted in diffusion rate control.

Mizoguchi and Habashi(27) studied the aqueous oxidation of complex sulphides containing ZnS, PbS and $CuFeS_2$ in hydrochloric acid and oxygen. The dissolution rate of the ZnS was found to be strongly dependent on agitation speed, and to have an activation energy of 15 kJ/mol, which differs considerably from the value of 90 kJ/mol reported by Rath *et al*, also in chloride solution. The complex sulphides studied by Mizoguchi and Habashi contained iron, which dissolved to some extent, thus ferric ions were present in their solutions, although probably at a lower concentration than was used by Rath *et al*(28), which may explain the difference in the observed kinetics of dissolution. Mizoguchi and Habashi concluded that the rate of ZnS dissolution was diffusion controlled. They also compared the dissolution of their sulphides in hydrochloric and sulphuric acids, and found dissolution to be significantly faster in hydrochloric acid than it was in sulphuric acid. This may explain the conclusion of diffusion control in chloride and chemical reaction control in sulphate systems(35, 36). The dissolution of ZnS in chloride systems may be fast enough to result in diffusion control, while in sulphate the slower rate may be caused by slower surface reactions.

Two more reviews of the studies carried out on oxidative leaching of sulphides are those of Woodcock(59) and Wadsworth(58).

Woodcock reviewed the work published prior to 1961, and discussed the oxidation of sulphides in terms of the properties of the given sulphide, the nature of the leaching solution, and the overall system, including temperature, agitation, and pulp density. Finally, Woodcock discussed the kinetics of the leaching reaction and the nature of the rate-limiting step. He quoted cases where the rate-controlling step was oxygen transfer to the leaching solution, transport across a diffusion barrier, transport through an insoluble film, heterogeneous reaction at the mineral surface, and mixed control. According to Woodcock, the reaction mechanism at the mineral surface can be regarded as an electrochemical process involving the simultaneous oxidation of the sulphide and reduction of the oxidant, analagous to the corrosion of metals. Wadsworth(57) reviewed the work published after 1961, and also pointed out the importance of electrochemical effects in sulphide leaching. He presented a generalised rate expression for the dissolution reaction, containing both transport and surface reactions, for which charge transfer may or may not be rate-controlling. Wadsworth used this generalised rate equation in a discussion of the dissolution of chalcopyrite, at the end of which he stated that the importance of electrochemical reactions in the dissolution of chalcopyrite is not clear form the observed kinetics which he reviewed.

The dissolution of chalcopyrite seems to differ from that of other copper minerals(58). Dutrizac(29) surveyed the literature on the ferric ion leaching of chalcopyrite, and undertook experimental work to resolve disputed points. He found the dissolution of chalcopyrite to be more rapid in chloride systems than in sulphate systems. The activation energy for chalcopyrite dissolution was found to be about 42 kJ/mol in chloride solutions and about 75 kJ/mol in sulphate systems. In both systems the dissolution rate was essentially independent of acid concentration and the intensity of agitation. The rate was found to be directly proportional to the available surface area in both chloride and sulphate systems. In sulphate systems, the addition of ferrous sulphate (and lithium and magnesium sulphates) substantially decreased the leaching rate. This was not the case for chloride systems, and the addition of chloride ion to a sulphate system accelerated the dissolution of chalcopyrite. In sulphate systems the dissolution rate was only slightly dependent on the ferric ion concentration, while in chloride

solutions the dependance was found to be greater. Parker, Paul and Power(61) presented an electrochemical explanation of the above observations. They postulated that a film of a metal-deficient polysulphide, which acts as a semiconductor, forms on chalcopyrite during oxidation. This film was believed to decompose thermally (achieving an equilibrium thickness) and to slow ion and electron transport, this being rate-limiting for much, but not all, leaching of chalcopyrite. Parker *et al* used their model to explain why the leaching rates were independent of agitation, why attrition grinding enhances the rate of dissolution of chalcopyrite, and the other effects reported by Dutrizac(29).

Lee and Donofrio(62) studied the leaching of chalcopyrite in hydrochloric acid and oxygen. They found that the rate-controlling step was chemical reaction at the mineral surface, and that the dissolution rate could be significantly enhanced by the addition of certain metals to the chalcopyrite. They attributed this effect to galvanic interaction between the metal and chalcopyrite particles resulting in the rapid conversion of chalcopyrite to chalcocite. Liddell and Bautista(63) modelled the dump leaching of chalcopyrite in terms of slow heterogeneous reaction between ferric ions and chalcopyrite and dissolved oxygen and chalcopyrite, and fast (pseudoequilibrium) formation of various sulphate complexes, such as $FeSO_4$, $FeHSO_4^+$, $FeOH^{2+}$, etc. They used their model to predict optimum conditions for the dump leaching of chalcopyrite. One result of this study was that raising the concentration of ferrous sulphate from 15,2 to 30,4 g/l (0,1 to 0,2 M) had a deleterious effect on the dissolution of chalcopyrite. Liddell *et al* explained this result in terms of the metal sulphate complexes present, and the earlier precipitation of $Fe(OH)_3$. However, Dutrizac(29) showed that up to concentrations of about 0,5 M, the addition of ferrous sulphate to ferric sulphate leach solution reduces the rate of dissolution of chalcopyrite. Therefore, the result of ferrous sulphate addition decreasing the dissolution rate of chalcopyrite is not as unexpected as Liddell *et al* considered, nor does it seem necessary to postulate ferric precipitation at the higher ferrous levels to explain the reduced dissolution rate.

A number of other reviews and studies of sulphide dissolution have been done. Habashi(60) and Majima(42) reviewed the electrochemistry of

sulphide dissolution in aqueous solutions. Habashi reviewed the historical development of aqueous metal sulphide dissolution, and described some commercial processes whereby metal sulphides are electrolysed to yield elemental sulphur and metallic products. Majima reviewed the literature on electrochemical processes occurring on sulphide surfaces. He found that electrochemical reactions seem to be especially important in acid solutions, and that in the most important cases, elemental sulphur is a product of anodic dissolution. The application of corrosion mechanisms was the main emphasis of Majima's review. He concluded that there is a need for much more research on, among other things, the stoichiometry and polarisation properties of electrochemical reactions of all important sulphide minerals and matte phases. Bolton(71) presented details of processes developed by Sherrit Gordon Mines for the oxidative pressure leaching of zinc and copper sulphides. Canterford and Dyson(26) studied the oxygen pressure leaching of mixed cobalt-nickel sulphides. Bolton and Canterford *et al* presented operating and experimental data only, without attempting any explanation of their results, apart from the reaction stoichiometry. Scott and Nicol(69) studied the dissolution in acid ferric sulphate of four different sphalerite concentrates. They concluded that the exact nature of the sphalerite had an appreciable effect on the kinetics of dissolution, and that both oxidative and non-oxidative mechanisms played a role in the dissolution of sphalerite. They suggested that more work was needed before a mechanism could be firmly established. Adams and Matthew(68) studied the leaching of zinc sulphide concentrates with mixtures of oxygen and sulphur dioxide in aqueous solution at atmospheric pressure. They found the rate of zinc extraction to be controlled by a surface chemical reaction, without interference from the sulphur product layer, for sulphur dioxide concentrations of up to nine percent in the gas phase. The dissolution kinetics were found to fit a shrinking core model, with an activation energy of about 155 kJ/mol, which is consistent with chemical reaction rate control. Hubli, Mukherjee and Gupta(67) presented experimental results of leaching nickel-copper sulphides in a ferrous chloride-oxygen system. They found that most of the copper and nickel could be solubilised, while most of the iron was eventually precipitated out of solution as a hydrated iron oxide. This was achieved by providing just

enough ferrous chloride in the initial solution to supply two chloride ions for each nickel or copper ion in the feed concentrate. Apart from the stoichiometry of the system, no attempt was made at explaining the experimental results. Grizo, Pacović, Poposka and Koneska(66) studied the leaching of a low-grade chalcocite-covellite ore in sulphuric acid in the presence of ferric ions leached from the ore, as a function of particle size, temperature and solution pH. They found three distinct phases in the dissolution kinetics. The first phase showed linear kinetics, and was ascribed to liquid phase mass transfer being controlling during the conversion of chalcocite to covellite. The second leaching period was thought to consist of mixed kinetics, while the third period, which again displayed linear kinetics was thought to be controlled by diffusion through product layers. The various measured activation energies were consistent with the rate-determining mechanisms assumed. Majima and Peters(65) compared the aqueous oxidation of a number of minerals, using oxygen at 120°C, by means of oxygen consumption *vs* time curves. The solutions were not assayed for dissolved metals, thus the effect of oxidation of sulphide sulphur to sulphate instead of elemental sulphur would tend to obscure the actual mineral dissolution. Nevertheless, the interesting observation was made that pyrrhotite exhibited very different dissolution behaviour at different solution pH values. In acid solutions pyrrhotite dissolved much faster than, for example, sphalerite or galena. In neutral solution, however, the pyrrhotite was found to leach more slowly than all the other sulphides tested. No explanation of the experimental observations was attempted.

A number of studies on the non-oxidative leaching of iron sulphides has been reported. Ingraham, Parsons and Cabri(73) studied the non-oxidative dissolution of pyrrhotite in hydrochloric acid. They concluded that nonstoichiometric pyrrhotite always produces an elemental sulphur residue, the amount of this residue being proportional to the non-stoichiometry of the pyrrhotite, that the leaching is rapid, and that the accumulation of the sulphur on the pyrrhotite surface retards the later stages of the leaching process. Dissolution of stoichiometric pyrrhotite (FeS, or troilite) produced no elemental sulphur. When air was allowed into the system during leaching, significantly more elemental sulphur was produced. No explanation of the leaching results

was attempted. Tewari and Campbell(74) studied the non-oxidative dissolution of troilite (FeS) in sulphuric acid. The rate of dissolution was found to depend on the acid and ferrous ion concentration in solution and the hydrogen sulphide partial pressure. A rate equation was presented, and it was concluded that the rate-controlling step was not transport of reactants or products. Nicol and Scott(75) studied the non-oxidative dissolution of some iron sulphides in acid solutions and found the kinetic data to be adequately explained by a reduction process followed by ionic charge transfer from a stoichiometric material. They used electrochemical theory to model the iron sulphide dissolution. Nicol(40) briefly reviewed the electrochemical theory of the dissolution of ionic solids, and showed that the non-oxidative leaching of oxides and sulphides can best be represented by the electrochemical model, rather than the various adsorption theories previously proposed. Nicol defined non-oxidative dissolution as dissolution in which the formal oxidation states of the various elements involved do not change during dissolution. Oxidative or reductive dissolution was defined as dissolution in which any of the solute species exist in different oxidation states in the solid and solution phases. Using these definitions, the dissolution of a sulphide MS can be said to be non-oxidative if the sulphur is liberated as hydrogen sulphide, and oxidative if elemental sulphur is produced.

Several studies have been reported on the oxidative leaching of iron sulphides. Björling and Gupta(77) studied the dissolution of artificial and natural pyrrhotite, chalcopyrite, sphalerite, molybdenite and galena in a mixture of nitric and sulphuric acid. They found that the iron in pyrrhotite could be transformed into an easily filterable ferric hydroxide precipitate, while impurities such as copper, nickel and cobalt remained in solution. A high yield of elemental sulphur was achieved. Björling and Gupta did not attempt to explain their results in terms of reaction rate mechanisms. Kunda, Rudyk and Mackiw(78) reported on the development of a process for the production of metallic iron and elemental sulphur from iron sulphides. One of the steps in this process was the aqueous oxidation of pyrrhotite in sulphuric acid and oxygen. They found that the most important factor controlling the rate of pyrrhotite oxidation was the mass transfer of oxygen from the gaseous phase to the mineral surface. Other

factors which affected the rate were temperature, initial sulphuric acid concentration, and the sulphur to iron ratio in the pyrrhotite. In a brief discussion of the leaching, Kunda *et al* presented stoichiometric relations for, among others, direct acid attack of the pyrrhotite and oxidation by reaction with ferric sulphates, i.e.,

a) $FeS + H_2SO_4 \rightarrow FeSO_4 + H_2S$

b) $FeS + Fe_2(SO_4)_3 \rightarrow 3FeSO_4 + S^o$

Gaseous oxygen plays no part in the above reactions, but is involved in the re-oxidation of ferrous to ferric sulphate and the oxidation of H_2S to elemental sulphur, as follows:

a) $2FeSO_4 + \frac{1}{2}O_2 + H_2SO_4 \rightarrow Fe_2(SO_4)_3 + H_2O$

b) $H_2S + \frac{1}{2}O_2 \rightarrow S^o + H_2O$

The overall stoichiometry, therefore, for both direct acid attack and reaction with ferric sulphate, is as follows:

$$FeS + \tfrac{1}{2}O_2 + H_2SO_4 \rightarrow FeSO_4 + S^o + H_2O$$

If this is so, then the observation that oxygen mass transfer is the most important factor in the oxidation of the pyrrhotite implies that, in this case, the transfer of oxygen from the gas to the liquid phase was the rate-limiting step, rather than transport of oxygen to the mineral surface, since oxygen was not involved in the solid-liquid dissolution reactions proposed. McKay and Halpern(79) studied the aqueous oxidation of pyrite in acid solutions by oxygen. They concluded that the rate of pyrite oxidation was controlled by a heterogeneous process on the mineral surface, involving oxygen. The pyrite sulphur was found to be converted to sulphate and elemental sulphur, the proportions depending on the leaching conditions. Subramanian, Stratigakos and Jennings(80) reviewed a number of hydrometallurgical processes for the recovery of iron, non-ferrous metals and sulphur from iron sulphide, and undertook experimental work, using an artificial pyrrhotite derived from thermal decomposition of pyrite, on some of the processes reviewed. They found that, when leaching the pyrrhotite in ferric sulphate, the resulting ferrous sulphate had no effect on the rate of leaching. However, no extraction *vs* time curves were given to substantiate this conclusion. Leaching in ferric chloride solution was found to be faster

than in ferric sulphate solution. No attempt was made at finding a rate equation for the pyrrhotite dissolution. Habashi(81) reported the results of pyrrhotite dissolution in nitric acid, and Thornhill(82) reported on laboratory and pilot plant testwork on the aqueous oxidation of pyrrhotite, using air. Neither of these two authors attempted to explain their results in terms of rate equations. Vezina(83) reported the results of a study of the effects of particle size distribution on the leaching of a pyrrhotite-pentlandite-chalcopyrite concentrate. Finer grinding was found to improve the leaching of the concentrate in oxygen. Explanation of the experimental results was not attempted.

Studies of a more fundamental nature have also been reported. Etienne(84) studied the copper-sulphur binary system in acid solution. He used electrochemical techniques to determine the copper activity for various copper sulphide compositions, and studied the growth of copper sulphide films on a copper anode in acidic solution saturated with H_2S. Etienne also measured current-potential curves for rotating discs of digenite and covellite, and related these polarisation curves to the electrolysis of copper matte anodes and leaching experiments in acid ferric sulphate solutions reported in the literature. This work was significant in that electrochemical theory was successfully related to oxidative acid leaching of copper sulphides. Brodie(1) and Paul, Nicol, Diggle and Saunders(2) studied the anodic dissolution of galena (PbS) in sulphate solution. They found the reaction to be electrochemical in nature, and proposed an electrochemical reaction mechanism which successfully predicted their observed current-potential curves. The reaction mechanism proposed consisted of two single-electron transfer steps, each controlled by electrochemical kinetics, one of them being an equilibrium reaction, as follows:

$$PbS \rightleftharpoons Pb^{2+} + S^{-} + e^{-}$$

$$S \rightarrow S^{o} + e^{-}$$

Therefore, overall:

$$PbS \rightarrow Pb^{2+} + S^{o} + 2e^{-}$$

The overall stoichiometry is in agreement with that in the literature for oxidative dissolution of metal sulphides. Corrans (ref. 32, pages 56 - 57) obtained current-potential curves for rotating discs of

pentlandite. The form of these curves can be simulated by electrochemical electron transfer kinetic equations, which indicates that pentlandite may also leach electrochemically.

In contrast to the electrochemical emphasis of the studies quoted above, studies have been published in which adsorption theories were used to explain the results of acid oxidative leaching of metal sulphides. Jan(33) concluded that the rate-determining step in the oxygen pressure leaching of sphalerite was the oxidation of H_2S at the sphalerite surface by the ferric ion. He found that the observed linear kinetics were due to the shape of the sphalerite particles, which in this case appeared to be in the form of flat plates, the surface area of which changed little during leaching. This may explain why Jan found linear kinetics for the leaching of his sample of sphalerite, while others(68) have found shrinking-core kinetics to be more applicable. In the latter case the sphalerite particles were probably approximately spherical, thus the surface area would change during leaching. Verbaan(35) studied the dissolution of sphalerite in acid ferric sulphate and in sulphuric acid solutions, and used Langmuir-Hinshelwood adsorption theories to explain his results. Verbaan conceded that electrokinetic phenomena may occur, but due to the difficulty of measuring these phenomena on sphalerite, he ignored them for the purposes of his thesis. In a later report, however, Verbaan(38) concluded that the leaching of sphalerite is electrochemical in nature. He reported on leaching experiments done on sphalerite in acid ferric sulphate solution, and presented an empirical correlation of his leaching results. Verbaan did not attempt to use electrochemical theory to form a rate equation for the leaching of sphalerite. Lowe(3) studied the initial rates of leaching of large single specimens of chalcocite, bornite, covellite, and pyrrhotite in acid ferric sulphate solutions. He obtained rate equations for each mineral and compared these equations to theoretical equations developed for various rate-controlling mechanisms, i.e., aqueous diffusion of ferric sulphate, solid-state diffusion of cuprous ions in the sulphide, chemisorption reactions and electrode processes. Because his experiments were not designed to investigate electrode processes, Lowe was not able to provide direct evidence for such processes. He did, however, show that the existence of such

processes was possible. Lowe's results for the dissolution of pyrrhotite were inconclusive. He conceded that a chemisorption mechanism similar to that proposed for bornite and covellite could exist for the ferric sulphate leaching of pyrrhotite, but found that the effects of temperature and acid concentration indicated departures from the chemisorption mechanism. Lowe suggested that these effects could have been caused by competition between direct acid attack of the iron sulphide, and ferric ion attack, i.e.,

$$Fe_2(SO_4)_3 + FeS \rightarrow 3FeSO_4 + S^o$$
$$H_2SO_4 + FeS \rightarrow FeSO_4 + H_2S$$

He recommended that additional test data should be measured before the mechanism of pyrrhotite leaching could be established.

Brittan(30) has proposed an empirical model for the leaching of low grade ores. He presented a variable activation energy model for the leaching reaction in which the various rate-limiting steps are lumped together into an arrhenius activation energy barrier which increases linearly with conversion. The reasoning behind this approach is that the more reactive material in an ore would dissolve more rapidly, leaving behind progressively more refractory material, thus corresponding to an increasing activation energy for the reaction as conversion progresses. Brittan fitted this model to the chloridization of oxide copper ore, and to the cyanidation of gold ore. In both cases the model fitted the experimental data very well. The trouble with such a model, however, is that it yields very little fundamental information about the leaching mechanism. This means that, although this model is mathematically simple (and therefore attractive), its use to extrapolate experimental results from, for example, laboratory to larger scale conditions, would be more risky than the use of a more fundamental model. In a given process, the various reaction resistances may occur in different proportions between small and large scale operation, which could result in poor prediction of the larger scale process. In a more fundamental approach, Loveday(31) presented a model for the leaching of an assemblage of non-porous particles, in which the bulk of the material is dissolved. This model illustrates the importance of properly accounting for the particle size distribution of the feed to a given leaching operation, if

the leaching kinetics are to be defined correctly. Loveday did not expand his model to account for changes in the leaching solution on the leaching kinetics. Roach and Prosser(34) have found that, when leaching low-grade ore where mass transfer is the rate-controlling step, the recovery of the desired species can be predicted from measured values of particle size, porosity, pore size and grain size of the valuable minerals, and constants available in the literature. Their approach requires a detailed knowledge of the ore mineralogy, and considers the effect of an inert matrix on the reactivity of mineral grains towards an external reagent. The problem in this case differs from metal sulphide leaching, because metal sulphide concentrates and mattes do not occur as grains in an inert matrix. Nevertheless, the idea of well-known mineralogy of the feed material fits in well with a fundamental study of sulphide leaching. There would be little point in doing fundamental studies on the rate of leaching of a given sulphide if its mineralogy were not known.

In summary, then, a considerable amount of literature has been published on the hydrometallurgical processing of metal sulphides. This literature review is by no means exhaustive, but it seems that most of the published work deals with the dissolution of copper and zinc sulphides. A number of studies have been published on the leaching of iron sulphide, but most of these presented experimental data with little or no theoretical interpretation of the results. One exception is the work of Lowe(3), although he was not able to conclusively establish the mechanism of dissolution of pyrrhotite in acid ferric sulphate solution. For copper and zinc sulphide leaching, various rate-controlling mechanisms have been proposed, including diffusion control and chemisorption and electrochemical rate-controlling steps. More recent publications on the leaching of copper and copper-iron sulphides seem to favour the electrochemical theory. Mao and Peters(85) studied the acid pressure leaching of chalcocite, and used an electrochemical mixed-potential model, coupled to shrinking-core, particle break-up and elemental sulphur morphology, to explain the observed kinetics. Warren Wadsworth and El-Raghy(86) used electrochemical theory to explain the anodic dissolution of chalcopyrite in sulphuric acid. Hillrichs, Grenlich and Bertram(87) investigated the electrochemical dissolution of copper and copper-iron sulphide ores in sulphuric acid, by means of

cyclic voltammetry. They interpreted their results in terms of the formation/dissolution kinetics of metastable surface layers. It seems significant that, in the Proceedings of the 3rd International Symposium on Hydrometallurgy (ref. 85 - 88), there are no papers which attempt to explain the kinetics of metal sulphide dissolution in terms of adsorption-desorption theories. Indeed, Wadsworth(88) gives, among others, the leaching of sulphide minerals as an example of electrochemical processes important in hydrometallurgy.

1.3 Scope of the present study

As reserves of high-grade base metal ores diminish and air pollution controls become stricter, manufacturers of base metals will probably be forced to consider hydrometallurgical processes. One such process is oxidative leaching of the low-grade (i.e. high iron) sulphides in sulphuric acid. This process has been examined previously (77, 78, 80, 81, 82, 83), but not in terms of the basic rate mechanism. Oxidative leaching decomposes metal sulphides as follows:

$$MS \rightarrow M^{2+} + S^{o} + 2e^{-}$$

Some of the oxidants reported in the literature are nitric acid, oxygen, ferric chloride and ferric sulphate. (The latter two being used in acid solution). Whatever the oxidant, the leaching solution will always contain dissolved iron, if iron-bearing sulphides are leached. In acid solution, ferric sulphate reacts with binary metal sulphides as follows:

$$MS + Fe_2(SO_4)_3 \rightarrow MSO_4 + 2FeSO_4 + S^{o}$$

(M = nickel, copper, cobalt, iron, etc.)

In oxygen pressure leaching the ferrous iron is re-oxidised to ferric iron as follows(78):

$$2FeSO_4 + \tfrac{1}{2}O_2 + H_2SO_4 \rightarrow Fe_2(SO_4)_3 + H_2O$$

Therefore, in simple ferric sulphate leaching, and in oxygen pressure leaching of low-grade sulphides, ferric sulphate plays an important part. An understanding of the mechanism of ferric sulphate dissolution of low-grade sulphide would be of great value if these processes were to become commercially significant. A reaction rate model, based on the correct

fundamental reaction mechanism, would facilitate accurate process design of full scale plant, and would thus be of great value.

Accordingly, this work is a study of the dissolution of a low grade matte in acid ferric sulphate solution. The overall objective of this study was to gain a fundamental understanding of the above leaching system, which may pave the way to fundamental understanding of more complex leaching systems, for example oxygen pressure leaching of sulphides in sulphuric acid, in the presence of ferric sulphate.

1.4 Criteria for a mathematical model

If a mathematical model of a leaching process is to be a useful tool for full-scale process design, it must account for the following factors:

a) Mineralogy and physical characteristics of the feed;
The minerals present in the feed material must be known. The feed particle size distribution must be known, along with the distribution of the various minerals between the particle sizes. The model must use this information as input data, and must be able to simulate the simultaneous leaching of different minerals.

b) Reaction mechanism:
The leaching model must be based on the correct fundamental reaction mechanism, which must predict the effects of changes in the leaching solution on the leaching rate. The appropriate rate-controlling step should be used.

c) Surface area change during leaching:
The effect of changing mineral surface area on the leaching rate must be predicted correctly.

d) Process design variables:
The model should be capable of accounting for the effects of variables such as temperature and agitation on the leaching rates.

The objective of this work was to produce a fundamentally sound mathematical model of the leaching of low-grade matte particles in acid ferric sulphate solution, which satisfies the above criteria.

2. EXPERIMENTAL

2.1 Description of matte

2.1.1 Mineralogy and chemical composition

The matte was divided into six fractions in a Warman cyclosizer. Tables 2.1 and 2.2 give the composition and relative amounts of each fraction. These six fractions were analysed by X-ray diffraction and electron microprobe. The X-ray diffraction data are shown in Appendix I.

The analyses revealed that the phases present in the matte were an iron-nickel alloy (metallic), troilite (FeS), a copper-iron sulphide and magnetite. The semi-quantitative analyses of these phases by electron microprobe are given in Table 2.3. In addition, detailed image analysis was used to find the quantitative amounts of each phase present in each size fraction. The results of this are given in Table 2.4. It was not possible to separate the copper-iron sulphide and the magnetite by image analysis, because they are optically very similar. Fortunately, however, it is not necessary to do so, because the data in Table 2.3 shows that no nickel is present in the magnetite or the copper-iron sulphide, no copper is present in the magnetite, and no cobalt in the copper-iron sulphide. This means that the magnetite plus copper-iron sulphide phase does not come into consideration for the leaching of nickel, and can be taken as one mineral phase for the leaching of copper. Magnetite is assumed to leach so slowly that it can be considered insoluble, thus the cobalt in the magnetite is taken to be insoluble as well. The leachable iron in the magnetite plus copper-iron sulphide is in the copper-iron sulphide only. The sulphide contains 16 per cent iron and 55,5 per cent copper (Table 2.3), while the magnetite has no copper. Thus all the copper is in the sulphide, and since the total copper and the ratio of copper to iron is known, the iron in the sulphide can be calculated.

Perry(23, page 3.13) gives the density of troilite as 4,84 g cm^{-3} and that of magnetite as 5,2 g cm^{-3}. Perry also gives a density of 7,4 g cm^{-3} for an alloy containing 30 per cent nickel (Ni-Resist type 3, page 23.38). This is roughly the amount of nickel in the alloy phase in the matte, thus the value of 7,4 g cm^{-3} was taken as the density of this alloy. The magnetite plus copper-iron sulphide phase was assumed to have the same density as pure magnetite. Since the

TABLE 2.1

Low grade matte : Chemical composition

Fraction	Composition, mass %			
	Ni	Cu	Co	Fe
1	1,88	2,73	0,12	56,0
2	2,77	2,17	0,14	58,3
3	3,02	2,01	0,15	58,0
4	3,10	1,84	0,16	58,1
5	3,40	1,74	0,18	58,6
6	5,12	1,94	0,25	59,3

TABLE 2.2

Low grade matte : Particle size distribution

Fraction	Particle size, microns	Mass %
1	less than 7,1	24,49
2	7,1 to 9,3	3,67
3	9,3 to 13,7	8,57
4	13,7 to 19,1	8,37
5	19,1 to 24,5	9,13
6	greater than 24,5	45,77

TABLE 2.3

Electron microprobe analysis of the matte phases

Phase	Composition, mass %			
	Fe	Ni	Co	Cu
Fe-Ni alloy	54-64	33-43	2,5-2,8	0,3-1,2
Troilite	59-62	0,3-1,9	0,4-1,1	0,2-1,5
Cu, Fe sulphide	13-19	0	0	51-60
Magnetite	70-71	0	0,7-0,8	0

TABLE 2.4

Volume proportions of each phase in matte size fractions

Fraction	Volumetric Proportions, %		
	Fe-Ni alloy	Troilite	Cu-Fe sulphide and magnetite
1	0,4	66,3	33,4
2	1,6	88,9	9,5
3	1,3	91,6	7,1
4	2,4	92,6	5,1
5	2,8	92,9	4,3
6	6,0	90,1	3,9

TABLE 2.1

Low grade matte : Chemical composition

Fraction	Composition, mass %			
	Ni	Cu	Co	Fe
1	1,88	2,73	0,12	56,0
2	2,77	2,17	0,14	58,3
3	3,02	2,01	0,15	58,0
4	3,10	1,84	0,16	58,1
5	3,40	1,74	0,18	58,6
6	5,12	1,94	0,25	59,3

TABLE 2.2

Low grade matte : Particle size distribution

Fraction	Particle size, microns	Mass %
1	less than 7,1	24,49
2	7,1 to 9,3	3,67
3	9,3 to 13,7	8,57
4	13,7 to 19,1	8,37
5	19,1 to 24,5	9,13
6	greater than 24,5	45,77

TABLE 2.3

Electron microprobe analysis of the matte phases

Phase	Composition, mass %			
	Fe	Ni	Co	Cu
Fe-Ni alloy	54-64	33-43	2,5-2,8	0,3-1,2
Troilite	59-62	0,3-1,9	0,4-1,1	0,2-1,5
Cu, Fe sulphide	13-19	0	0	51-60
Magnetite	70-71	0	0,7-0,8	0

TABLE 2.4

Volume proportions of each phase in matte size fractions

Fraction	Volumetric Proportions, %		
	Fe-Ni alloy	Troilite	Cu-Fe sulphide and magnetite
1	0,4	66,3	33,4
2	1,6	88,9	9,5
3	1,3	91,6	7,1
4	2,4	92,6	5,1
5	2,8	92,9	4,3
6	6,0	90,1	3,9

densities of chalcopyrite ($CuFeS_2$, 4,1 - 4,3 g cm^{-3}) and bornite (Cu_5FeS_2, 4,9 - 5,4 g cm^{-3}) range around that of magnetite(25) this is a reasonable assumption.

Using the above densities, the measured volumetric phase proportions shown in Table 2.4 can be converted to mass proportions, which are shown in Table 2.5. Now, since the mass proportion of the various phases have been calculated, and composition ranges for nickel, copper, cobalt and iron for each phase have been measured, values inside these ranges can be assigned to the nickel, copper, cobalt and iron content of each phase. This is done by searching for the set of values for the nickel, copper, cobalt and iron content of each phase, within the measured ranges, that best predicts the overall composition of each size fraction. One way of performing this search is to define an error function as the sum of the squared differences between the measured and calculated overall compositions of the different matte size fractions. The calculated overall compositions are found by using the mass phase proportions in Table 2.5, and the current values of nickel, copper, cobalt or iron composition of each phase. The first and second partial derivatives of the error function, with respect to the nickel, copper, cobalt or iron composition of each phase are then used to find the minimum squared difference between calculated and measured overall compositions. At this minimum, all the partial first derivatives are zero, and all the partial second derivatives are positive.

A Fortran V computer programme was written to do the above search, and solved on an Eclipse S250 computer. The programme is shown in Appendix IX. Once the nickel, copper cobalt and iron compositions were found, the programme calculated the per cent distribution of nickel, copper, cobalt or iron in the various phases. The print-outs of these calculations are shown in Appendix I, and the calculated proportions in each phase are given in Tables 2.6 to 2.9. The leachable iron in the magnetite plus copper-iron sulphide phase is the iron associated with the copper in the copper-iron sulphide.

TABLE 2.5

Mass proportions of each phase in the matte size fractions

Fraction	Mass Proportions, %		
	Fe-Ni alloy	Troilite	Cu-Fe sulphide and magnetite
1	0,6	64,6	34,8
2	2,4	87,6	10,0
3	2,0	90,5	7,5
4	3,6	91,0	5,4
5	4,2	91,3	4,5
6	8,9	87,1	4,0

TABLE 2.6

Proportions of nickel in matte phases

Fraction	Proportions, % of total in fraction		
	Fe-Ni alloy	Troilite	Cu-Fe sulphide and magnetite
1	16,5	83,5	0
2	36,8	63,2	0
3	32,0	68,0	0
4	45,7	54,3	0
5	49,4	50,6	0
6	68,5	31,5	0

TABLE 2.7

Proportions of copper in matte phases

Fraction	Proportions, % of total in fraction		
	Fe-Ni alloy	Troilite	Cu-Fe sulphide and magnetite
1	0,25	33,22	66,53
2	1,52	69,14	29,34
3	1,33	75,43	23,24
4	2,53	79,86	17,62
5	3,02	81,96	15,02
6	6,53	79,84	13,63

TABLE 2.8

Proportions of cobalt in matte phases

Fraction	Proportions, % of total in fraction		
	Fe-Ni alloy	Troilite	Cu-Fe sulphide and magnetite
1	8,24	59,07	32,69
2	27,16	65,27	7,57
3	23,23	70,78	5,99
4	36,11	60,25	3,64
5	39,88	57,23	2,89
6	59,66	38,68	1,66

TABLE 2.9

Proportions of iron in matte phases

Fraction	Proportions, % of total in fraction			
	Fe-Ni alloy	Troilite	Cu-Fe sulphide and magnetite	
			Soluble	Insoluble
1	0,67	68,20	1,88	29,25
2	2,58	88,83	0,52	8,07
3	2,14	91,44	0,39	6,03
4	3,84	91,55	0,28	4,33
5	4,48	91,69	0,23	3,60
6	9,45	87,16	0,20	3,19

2.1.2 Particle size distribution

A Leeds and Northrup Microtrac particle size analyser was used to measure the particle size distribution of four samples of the matte. The average of these four distributions is shown in Figure 2.1, and the individual results are given in Appendix I. The average particle size distribution from the microtrac results differs from that obtained from the Warman cyclosizer (Table 2.2). The microtrac measures individual particle sizes optically (i.e., a laser beam), while the cyclosizer separates particles of differing size or density by means of hydrocyclones. Since these two techniques use such different methods of particle size measurement, one may expect them to yield somewhat different results.

The microtrac results span a larger part of the total matte than the cyclosizer results, therefore the microtrac particle size analysis was used. Because the mineral proportions in the matte change with increasing particle size, and this change was measured in the six size fractions from the cyclosizer, these size fractions were assigned size ranges by projecting the cumulative cyclosizer per cent undersize values onto the microtrac curve, and reading off the corresponding particle sizes. The cyclosizer fractions 1 and 6, which account for about 24 and 46 per cent of the matte respectively, were subdivided into smaller fractions using the microtrac size distribution curve. The final "average size" fractions used to represent the matte are as follows:

Particle size, microns			Mass %	Remarks
Lower	Upper	Average		
0	2,8	2,4	6,83	Cyclosizer fraction 1
2,8	3,9	3,3	6,80	
3,9	5,6	4,6	10,86	
5,6	6,5	5,7	3,67	Cyclosizer fraction 2
6,5	9,0	7,1	8,57	Cyclosizer fraction 3
9,0	12,5	10,1	8,37	Cyclosizer fraction 4
12,5	16,0	13,9	9,13	Cyclosizer fraction 5

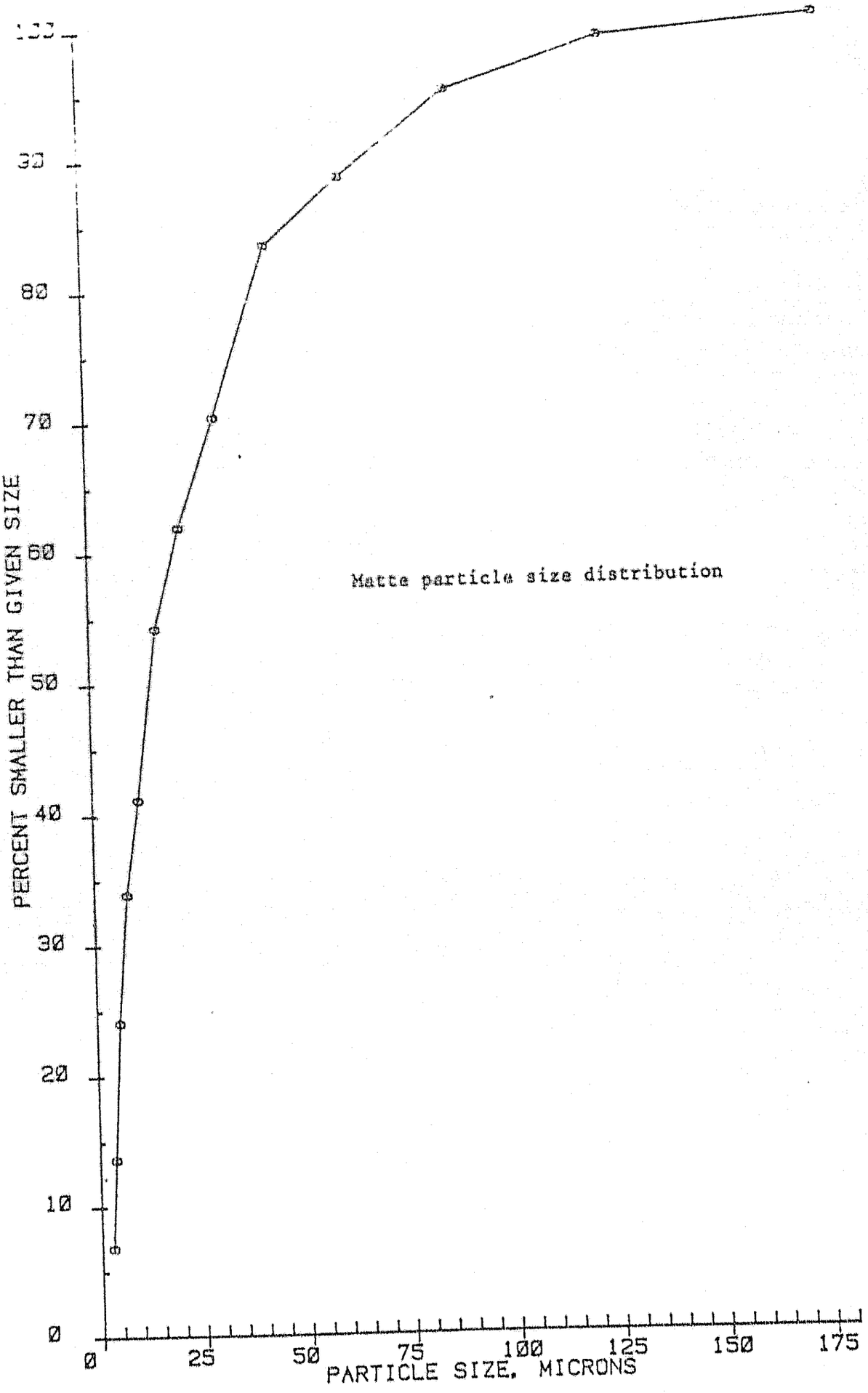

Matte particle size distribution
PERCENT SMALLER THAN GIVEN SIZE
80
70
60
50
40
30
20
10
0
0
25
50
75
100
125
150
175
PARTICLE SIZE, MICRONS

Fig. 2.1

Particle size, microns			Mass %	Remarks
Lower	Upper	Average		
16	22	18,8	7,70	Cyclosizer fraction 6
22	31	26,1	8,38	
31	44	36,9	13,08	
44	62	52,2	5,05	
62	88	73,9	6,55	
88	176	105	5,03	

The mineral proportions for each size range were assigned according to the measurements done on each cyclosizer fraction, as described previously.

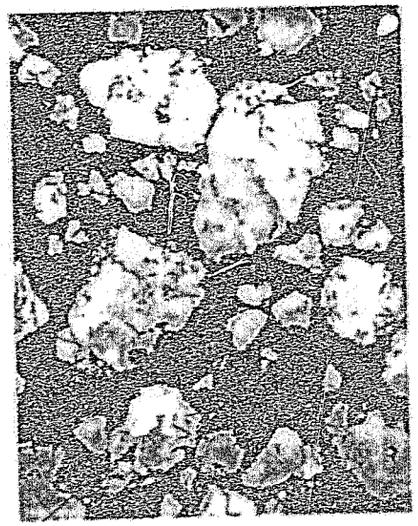
2 1.3 Physical appearance

Plates I and II are photomicrographs of the matte. The whitish areas in the particles are the iron-nickel alloy, the light grey areas are troilite (iron sulphide) and the dark grey areas are magnetite plus a copper-iron sulphide.

Plate I shows micrographs of the coarse fraction (cyclosizer fraction 6) of the matte. The major phase present is the troilite, with the alloy and copper, iron sulphide plus magnetite phases present as inclusions in the troilite. The alloy inclusions vary in size, but they are only rarely much smaller than the troilite grains in which they reside. In most cases, the alloy is not encapsulated in the troilite. Not all of the troilite grains contain alloy. The copper, iron sulphide plus magnetite phase occurs as very small inclusions in the troilite grains, mostly fully enclosed. Again, not all of the troilite grains contain these inclusions.

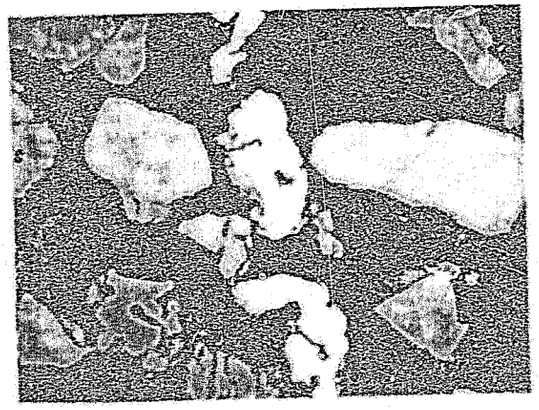
Plate II shows cyclosizer fractions 5 and 2 at higher magnification than plate 1. Where a particle in fraction 5 contains alloy, the alloy grain is of similar size to the particle, and is not encapsulated in the troilite. The copper-iron sulphide plus magnetite phase occurs as inclusions in the troilite, which are mostly not fully encapsulated in the troilite. Only some of the troilite grains contain inclusions of the other phases. In fraction 2 the phases appear to be of similar size, and exposed in those grains which contain more than one phase.



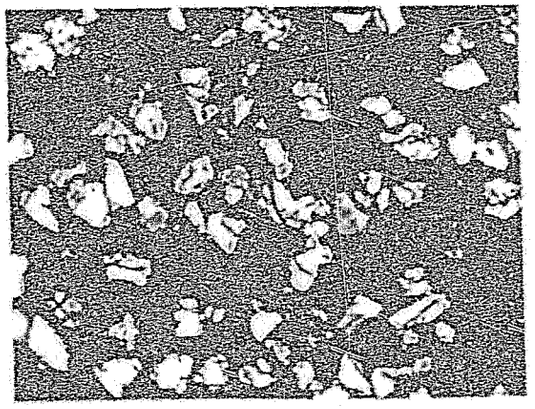


50 microns

PLATE I: Photomicrographs of cyclomizer fraction 6 of the matte



Fraction 4



Fraction 5

50 microns

PLATE II: Photomicrographs of cyclosizer fractions 4 and 5 of the matte

In the micrographs in plates I and II, the particles have irregularly rounded shapes. Needles or flat-plate types of particle shapes are not evident in the matte.

2.1.4 Degree of liberation of sulphide phases from alloy phase

The micrographs in plates I and II show that, although the alloy does not occur as separate particles, the sulphide grains do not all contain alloy inclusions. To obtain a rough idea of the amount of the sulphide containing alloy inclusions, consider a large number of matte particles, some of which contain alloy inclusions, others of which do not. The following rough calculation can be made:

Total number of particles present	:	N
Number of particles containing alloy	:	n
Particles containing alloy: volume fraction alloy:		x
Overall volume fraction alloy (whole sample)	:	X

The overall volume fraction of alloy is given by :

$$X = \frac{n}{N} x$$

Therefore: $n/N = X/x$ = fraction of particles containing alloy.

The fraction of the sulphide in the mixed particles is given by:

$$F = \frac{n(1 - x)}{N}$$ = fraction of sulphide associated with alloy inclusions.

Now consider the different cyclosizer fractions of matte. Fraction 6 (coarsest fraction) comprises about 46 per cent of the matte, and contains 6,0 per cent by volume of alloy. Examination of plate I shows that most of the alloy is present in this fraction as inclusions occupying roughly between one half and one fifth of the individual particle volumes. In terms of the above derivation, this gives:

x = 0,5 to 0,2

X = 0,06

Thus n/N = 0,12 to 0,30

and F = 0,06 to 0,24

As a check on this calculation, a polished section of cyclosizer fraction 6 was studied under a microscope, and individual particles were counted. Of the 332 particles counted, 91 contained visible alloy inclusions. This translates into a value of 0,27 for the fraction n /N above, which is within the calculated range.

Examination of plate II shows that, for cyclosizer fraction 5, the volume of alloy, in those grains containing alloy, is roughly between 50% and 80% of the particle volume. For fraction 2, these proportions seem to be roughly the same as for fraction 5, thus it can safely be assumed that they hold for fractions 5 to 1.

Using these assumptions, and the above procedure, the following numbers can be calculated for each cyclosizer fraction:

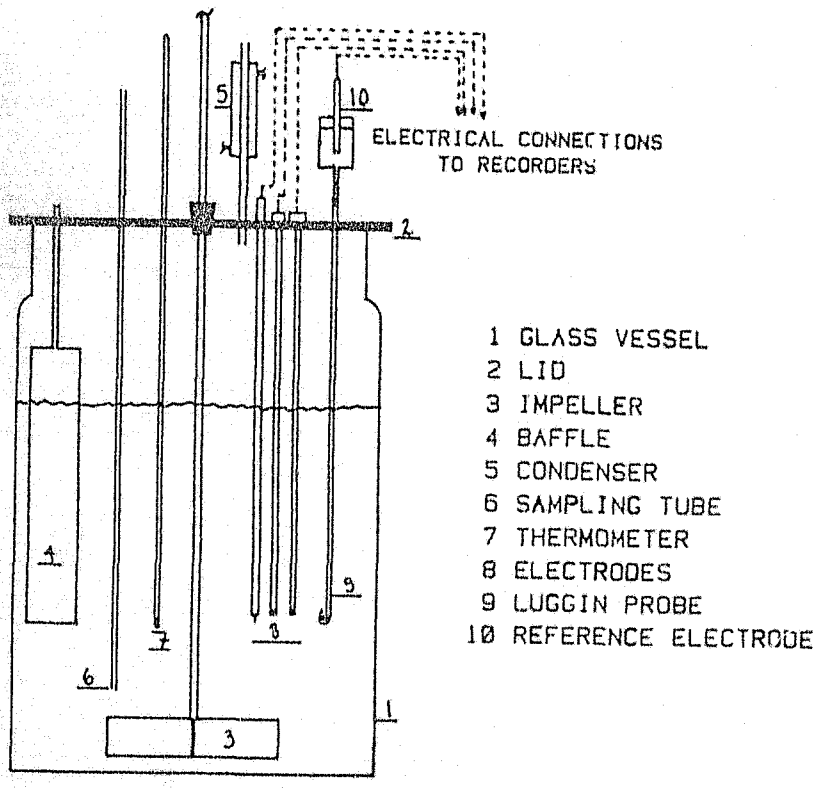
Fraction number	M- %	% Sulphide associated with alloy
6	45,77	6 to 24
5	9,13	0,7 to 2,8
4	8,37	0,6 to 2,4
3	8,57	0,3 to 1,3
2	3,67	0,4 to 1,6
1	24,49	0,1 to 0,4

Summation over the six fractions of the mass per cent of each fraction, times the per cent sulphide associated with alloy in the fraction, gives the amount of troilite associated with alloy in the total matte. This yields a value of between 2,9 per cent and 11,7 per cent, which means that at least 88 per cent of the sulphide in the matte is not associated with alloy, i.e., is "fully liberated" from the alloy, in terms of galvanic interaction (See section 4.1.(d)).

2.2 Leaching of matte

2.2.1 Leaching apparatus

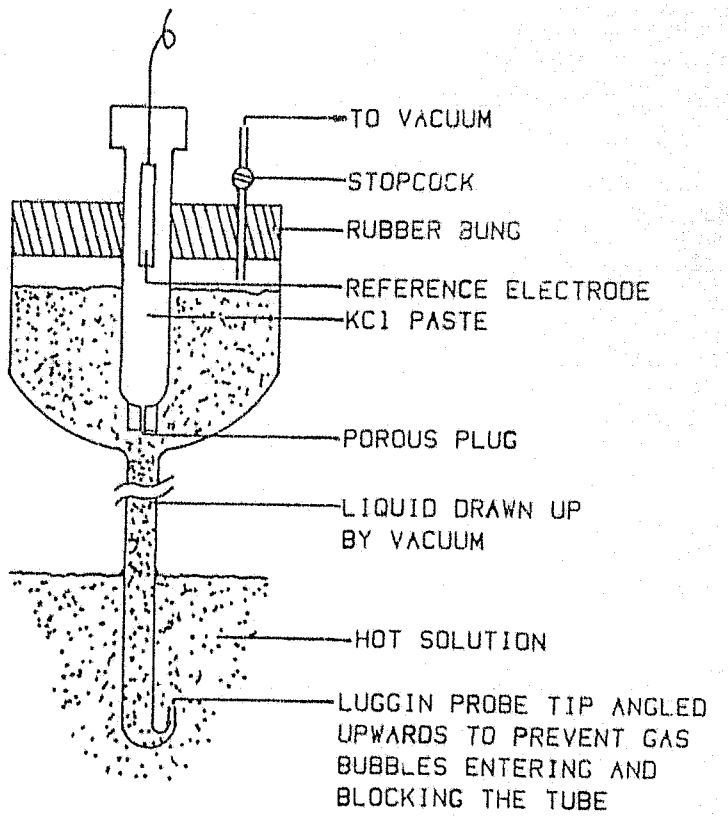
The leaching experiments were conducted in a two litre, flat bottom, cylindrical, flanged, glass reaction vessel. Figure 2.2(a) is a



1 GLASS VESSEL
2 LID
3 IMPELLER
4 BAFFLE
5 CONDENSER
6 SAMPLING TUBE
7 THERMOMETER
8 ELECTRODES
9 LUGGIN PROBE
10 REFERENCE ELECTRODE

DIAGRAM OF THE LEACH REACTOR

Fig 2.2 (a)



LUGGIN PROBE AND REFERENCE ELECTRODE

Fig 2.2 (b)

diagram of the reaction vessel and its internals. The vessel was equipped with a flat stainless steel lid, with one central port, and eight other ports in a circle around the central one. Agitation was supplied by a stainless steel flat four-bladed turbine, driven via a flexible drive cable by a variable speed electric motor. The vessel internals consisted of a perspex baffle, a thermometer and a sampling tube. A nitrogen purge was supplied from a high pressure cylinder, via a pressure regulator and a rotameter, through the resampling tube. The vessel was vented through a condenser. The reaction vessel was heated in an oil bath, and the heater in the oil bath was controlled by a contact thermometer.

For the leaches during which potential measurements were taken, a luggin probe, a platinum electrode, and two other electrodes, made from fresh matte and leached residue respectively, were inserted in the reactor. A saturated calomel electrode (S.C.E.) was connected to the luggin probe, as shown in figure 2.2(b). Potentials were recorded on two Leeds and Northrup Speedomax two pen chart recorders.

2.2.2 Matte and residue electrodes

The fresh matte and leached residue electrodes were made by compressing about one gram of matte or residue at a pressure of 7,5 tonnes/cm^2 in a Paul Weber KBr die and press. A wire was fixed to the resulting disc by a silver-bearing conducting epoxy resin (ECCOBOND V 91, Emerson and Cuming Europe NV). Once this resin had set, the disc was suspended above a high temperature resin (ARALDITE CW216) inside an evacuated glass vessel, then lowered into the resin. Once the disc was fully immersed in the resin, the vacuum was broken. The disc was left in the resin for a few minutes to allow the resin to penetrate as far as possible into the pores of the disc. Before the resin set, the disc was removed and mounted in a teflon holder. The electrode was then cured at about 90 degrees C in an oven for two hours. Once cured, the electrode face was ground with emery paper (1000 grit) on a polishing wheel, to expose the mineral surface. The electrode plus holder were then fixed to a second long holder using the same high temperature epoxy as before and again cured at about 90°C for two hours. The electrode was then ready for use. Figure 2.3 shows a sketch of this type of electrode.

MATTE ELECTRODE

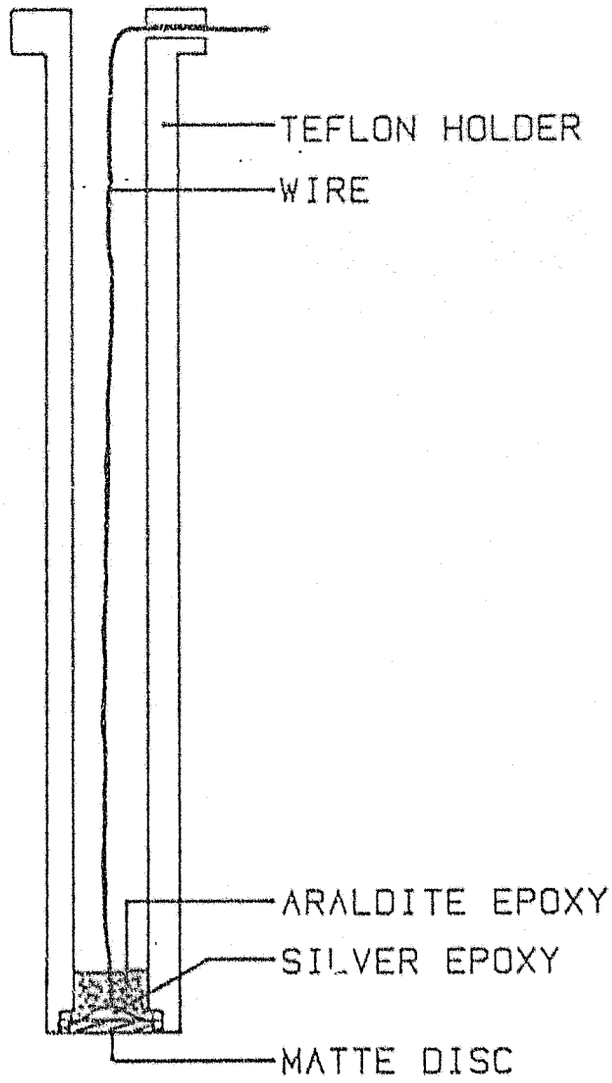


Fig 2.3

2.2.3 Leach solution

For each group of leaching experiments, a sufficient quantity of fresh leach solution was made up and kept in a large closed glass bottle. Leach solution for each experiment was taken from this bottle when required, thus a given group of leach runs used exactly the same starting solution.

The leaching solution was made up by dissolving ferric sulphate powder (A.R. grade) in deionised water, and adding concentrated sulphuric acid (98 per cent H_2SO_4) to aid the dissolution of the ferric sulphate. The solution contained approximately 100 grams per litre of Fe^{3+}, and about 90 grams per litre of H_2SO_4.

2.2.4 Leaching procedure

For each leaching experiment, 1,5 litres of the ferric sulphate solution was poured into the leaching vessel, and the vessel was put into the oil bath. The stirrer drive was connected to the impeller shaft, and the condenser to the vessel lid. Cold liquid was drawn up the luggin probe to cover the tip of the reference electrode, by vacuum. (Where potential was not recorded, this last step was obviously not done.) The oil bath heater and the leach vessel stirrer were switched on, and cooling water flow to the condenser and the nitrogen purge were started. When the temperature of the leach solution had stabilised at 90°C, the leach was started. Ten grams of matte was weighed out on waxed weighing paper, to within $\pm$ 0,01 grams accuracy, on an electronic balance. This matte was poured from the weighing paper into the leach vessel. It took about five to ten seconds to pour all the matte into the leach vessel. When potential was to be measured, the matte and residue electrodes were inserted into the solution immediately after the matte was poured into the reactor. Time zero was taken as the start of pouring the matte into the vessel. Samples were drawn through the sampling tube into a small sample holder by vacuum, then filtered under pressure in a small stainless steel pressure filter, using 0,2 micron filter membranes. Solids from the filter were combined for assay for the overall material balance. The filtered liquid samples were cooled and their volumes were recorded. The sampling tube was kept clear

of liquid between sampling by means of the nitrogen purge, thus dead volume in the sampling tube was avoided. Samples were taken at six, fifteen, thirty and sixty minutes after the start of leaching, and thereafter at hourly intervals to the end of the leach - usually a total time of seven hours. After each sample, the small pressure filter was thoroughly rinsed with deionised water, then dried. The washings were collected, the total volume recorded, and assayed for inclusion in the overall material balance.

On completion of the leaching experiment, the leach vessel was removed from the oil bath, and the contents were filtered hot in a larger rubber-lined pressure filter, using Whatman no. 542 filter paper as the filter medium. The leach vessel and internals were thoroughly rinsed with deionised water. The wash water from this rinse was filtered and kept for analysis. The solids from the rinse were combined with the solids from the leach solution. This leach residue was washed by three displacement washes of deionised water in the pressure filter, then dried and weighed for analysis. The displacement wash water was combined with the vessel rinse water for analysis.

2.2.5 Sample analysis

The leach solution samples taken during and after the leaches were analysed for ferrous iron by titration with potassium dichromate. Analysis of the leach solutions for nickel, copper, cobalt, total iron and sulphate was done by inductively couples plasma atomic emission spectrometry (ICP-AES). Wash water samples were analysed for nickel, copper, cobalt and total iron in the same way.

Solid samples were fused with sodium peroxide, dissolved and analysed by ICP-AES, as for the liquid samples.

2.2.6 Calculation of extractions during leaching

a) Ni, Cu, Co

The extraction of Ni, Cu and Co during any given leach were calculated as follows:

i) Overall extraction = X

$$X = \frac{V_f(C_f - C_i)}{V_f(C_f - C_i) + R}$$

Where: V_f = Volume of pregnant liquor out, litres

C_f = Concentration of Ni, Cu, or Co in pregnant liquor, mg/l

C_i = Concentration of Ni, Cu or Co in initial leach liquor, mg/l

R = Mass of Ni, Cu or Co in the solid residue filtered from the pregnant liquor, mg.

ii) Extractions during leaching = x(t)

$$x(t) = \frac{X(C(t) - C_i)}{(C_f - C_i)}$$

Where: C(t) = Concentration of Ni, Cu or Co in the sample taken at time t, mg/l

b) Fe

Since the initial total iron concentration in the leach solution was much higher than the change in total iron concentration during leaching, the above method could not be used to calculate the iron extraction vs time curves. Instead, these curves were calculated from the ferrous iron concentrations, which changed sufficiently during leaching for accurate calculations to be possible.

The leaching reaction involved is:

Sulphide: $MS + 2Fe^{3+} \rightarrow M^{2+} + 2Fe^{2+} + S^{o}$

Alloy : $M + 2Fe^{3+} \rightarrow M^{2+} + 2Fe^{2+}$

Where: M = Ni, Cu, Co or Fe

Thus, for every mole of M leached, two moles of ferric ions are reduced to ferrous ions. Once the extractions of Ni, Cu and Co have been found, the amount of ferrous ions generated by the dissolution of Ni, Cu and Co can be calculated and subtracted from the total amount of ferrous ions generated by the dissolution of Ni, Cu, Co and Fe. The difference is the amount of ferrous ions generated by dissolution of iron - for each

mole of iron leached, three moles of ferrous ions appear in the solution. This enables the accurate calculation of the amount of iron dissolved, and thus the iron extraction can be calculated similarly to the extractions of Ni, Cu and Co.

2.2.7 Leaching conditions

a) Temperature, pressure and stirrer speed

All the leaches were done under atmospheric pressure, at a stirrer speed of 600 r.p.m. Leaches were done at 90°C, 52°C, 28°C and 25°C. The upper two temperatures were constant to within ± 0,5°C, and the lower two were constant to ± 1°C.

b) Initial solution composition

The initial leaching solution compositions are summarised in Table 2.10. The first three leaches were done to check the reproducibility of the leaching results. The next three leaches tested the effect on leaching rates of ferrous iron concentration, and the following two were run in order to measure the potentials of electrodes made from fresh matte and leached residue, during leaching. The last three leaches were performed to investigate the effect of temperature on the leaching rates.

2.3 Measurement of solution redox potential

2.3.1 Apparatus

The equipment used for the measurement of the solution redox potential was the same as that used for the leaching experiments. The leach vessel was fitted with a platinum electrode in the hot solution, and the reference saturated calomel electrode and luggin probe, as shown in Figure 2.2. The potential difference between these two electrodes was measured with a high-impedance voltmeter.

2.3.2 Procedure

a) Measurement at 90°C

Two experiments were done, both starting with solution of the same composition as that used in leaches 1 to 5. The initial solution - 1,5 litres - was heated to 90°C in the leach vessel, in the same way as for

TABLE 2.10

Initial leaching solution compositions

Leach number	Concentration, mg/l			Concentration, g/l		
	Ni	Cu	Co	Fe^{2+}	Fe^{3+}	$SO_4^{=}$
1	22	1	5	0	101,2	
2	22,8	1,92	4,90	0	102,7	
3	22,8	1,88	4,99	0	101,3	
4	31,1	1,46	6,43	6,94	102,9	
5	33,7	3,75	7,61	18,69	96,6	
6	37,8	4,33	9,14	33,63	126,9	
7	33,7	1,42	7,80	0,03	99,8	292
8	33,7	1,42	7,80	0,03	99,8	292
9	11,9	1,33	2,82	0	118,0	355
10	12,4	2,24	3,15	0	118,0	355
11	8,2	1,21	2,02	0	101,0	300

the leaching experiments. In the first experiment (Experiment A), solid ferrous sulphate ($FeSO_4 \cdot 7H_2O$), of A.R. grade, was added in increments to the hot solution. In the second experiment (Experiment B), finely powdered elemental iron was used, instead of ferrous sulphate. After each addition of iron or ferrous sulphate, the solution potential was allowed to stabilise, and was then recorded, and a liquid sample was withdrawn for analysis. In the experiment which used iron powder, the liquid samples were immediately filtered in the small stainless steel pressure filter, to remove any traces of iron particles which may have still been slowly dissolving.

b) Measurement at 22°C

A set of eighteen solutions was made up, using ferrous and ferric sulphate (A.R. grade) and sulphuric acid. The compositions of these solutions is given in Appendix III. Redox potentials were measured by dipping the platinum and reference (calomel) electrode into the various solutions and waiting till the voltmeter reading stabilised before noting the potential. To prevent distortion of the solution compositions, the electrodes were rinsed in deionised water and dried before being placed in the next solution The solution temperatures were all 22°C during these measurements.

2.4 Electrochemical measurement of matte leaching rate as a function of potential

2.4.1 Apparatus

The same leaching vessel was used as for the leaching experiments. A new matte electrode was made for this experiment. Three electrodes were used, i.e. the matte electrode as the working electrode, the platinum electrode as a counter electrode, and the saturated calomel electrode as the reference electrode. For this experiment, a new luggin probe was made. The matte electrode face rested on the tip of this new luggin probe. Figure 2.4 shows a sketch of this probe. The electrodes were connected to a potentiostat. The potentiostat could apply any required potential, relative to the reference electrode, to the working electrode, and was equipped with an ammeter for the measurement of the current passing to the working electrode. Figure 2.5 is a diagram of the experimental set-up.

2.4.2 Procedure

A 1,5 litre solution was made up, containing 380 grams per litre of sodium sulphate, and 67 grams per litre of sulphuric acid. This solution was heated in the leach vessel in the same way as at the start of the leach experiments. Once the solution temperature had stabilised at 90°C, the stirrer was switched off, the electrode was inserted into the solution, and a current of about 10 milliamps was passed through the electrode for about an hour, to remove the alloy fraction from the electrode face. Next, the matte electrode potential, relative to the reference electrode, was brought to 250 mV and the current was allowed to stabilise, then recorded. The matte electrode potential was then increased by 50 millivolts, the current was allowed to stabilise and was then recorded. This procedure was repeated up to a measured electrode potential of 650 millivolts.

LUGGIN PROBE AND MATTE
ELECTRODE
ELECTROCHEMICAL EQUIPMENT

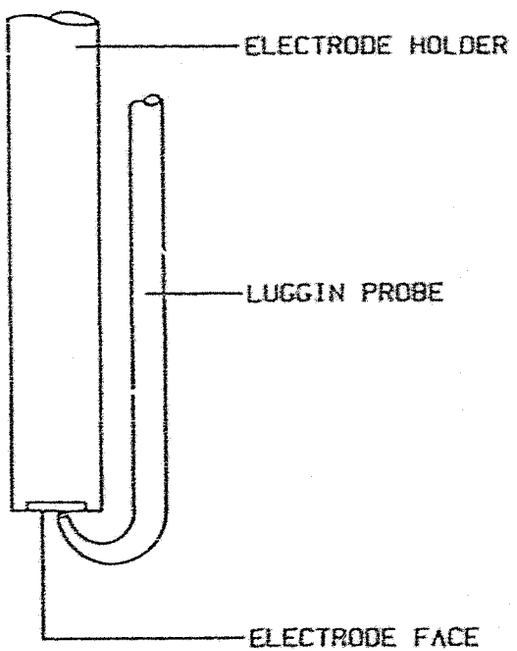


Fig 2.4

ELECTROCHEMICAL SET-UP

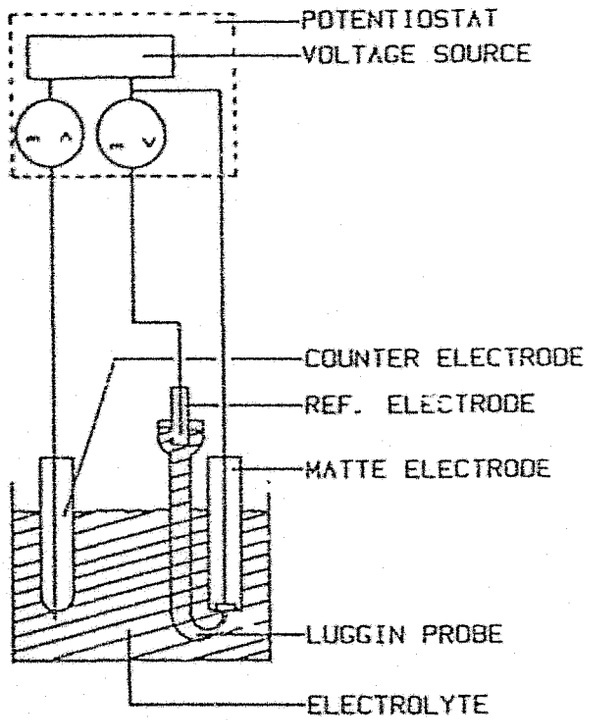


Fig 2.5

LUGGIN PROBE AND MATTE ELECTRODE FOR THE ELECTROCHEMICAL EXPERIMENT

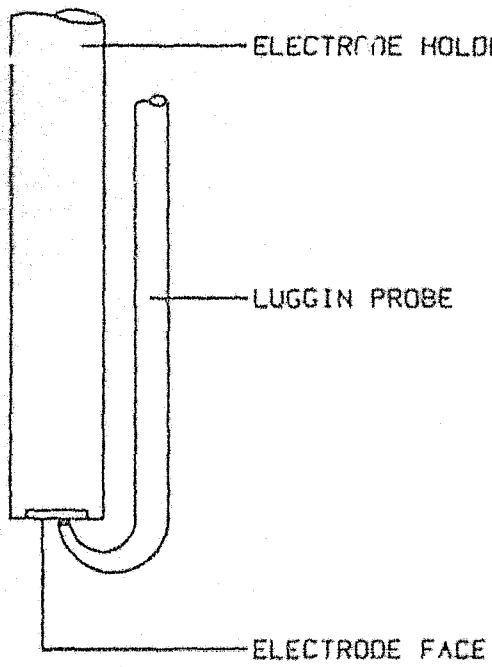


Fig 2.4

ELECTROCHEMICAL SET-UP

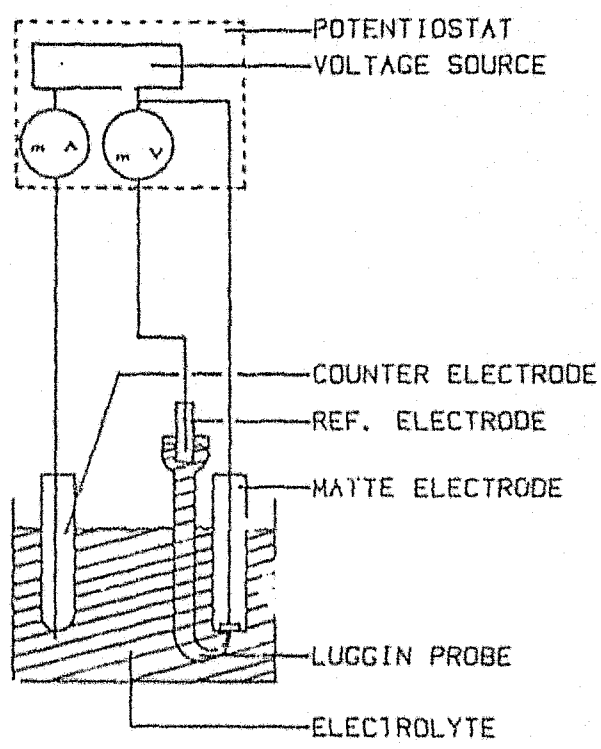


Fig 2.5

3. RESULTS

3.1 Leaching of matte

The results of the leaching experiments are summarised in Figure 3.1. The full results, including material balances for the leaching experiments, are given in Appendix II.

Figure 3.1 shows typical extraction *vs.* time curves for the leaching of the base metals, as well as potentials recorded during leaching. The extraction of a metal from the matte is defined as follows:

$$X_M = \frac{\text{Amount of M dissolved from matte}}{\text{Amount of M in original unleached matte}}$$

where X_M is the extraction of metal M, and M is nickel, copper, cobalt, or iron.

Figure 3.1(a) and (b) shows the results of leaches 1 to 3 for nickel and iron. These leaches used the same experimental conditions, thus these results show the degree of reproducibility obtained in the leaching experiments. Similar results were obtained for copper and cobalt. The maximum difference between extraction *vs.* time curves for iron is 0,05. The curves for nickel and copper differ by 0,05 or less, except for one point, at fifteen minutes after the start of leaching. The differences at this point are less than 0,06. The curves for copper differ by more than 0,05 at two points only, at fifteen minutes and five hours after the start of leaching, the differences in this case being 0,07 at fifteen minutes and 0,06 at five hours after the start of leaching.

Figure 3.1(c) and (d) shows the effect on the leaching rates of the addition of ferrous ions to the leaching solution prior to the start of the leach, for nickel and iron. Leach 3 had no ferrous ions added to the initial leach solution. Leaches 4, 5 and 6 had increasing amounts of ferrous ions added to the initial solution, as follows:

Leach no.	Initial Fe^{2+} concentration, g/l
3	0
4	6,9
5	18,7
6	33

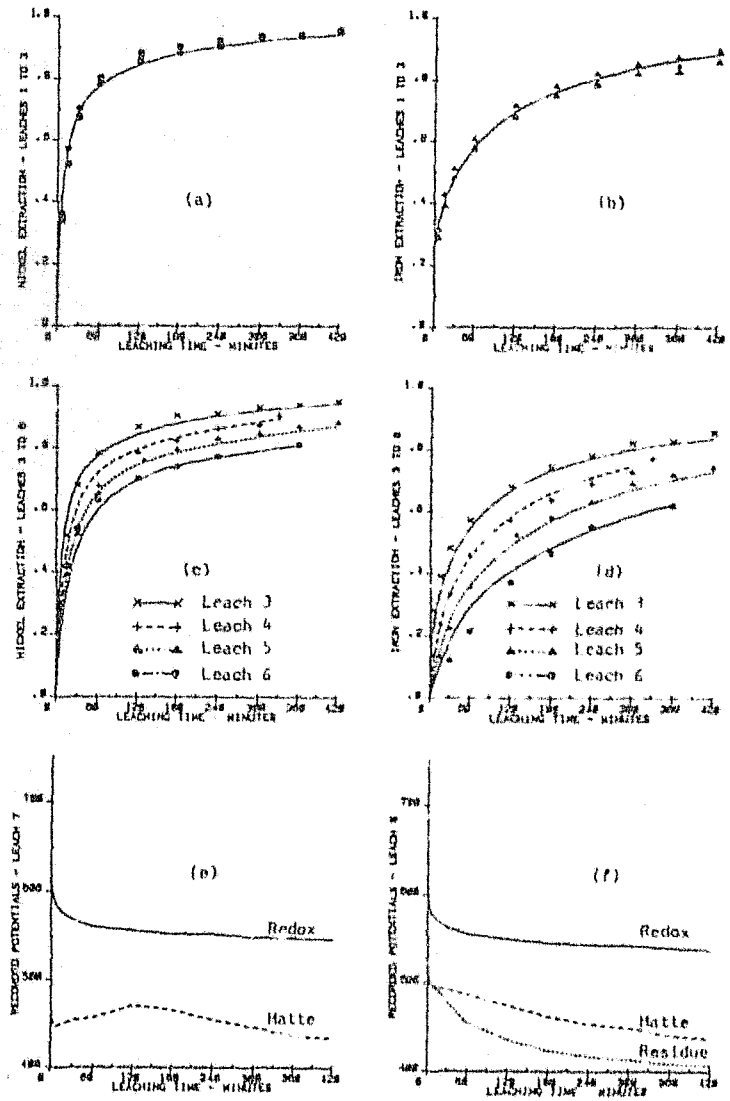


Fig. 3.1 Typical experimental results

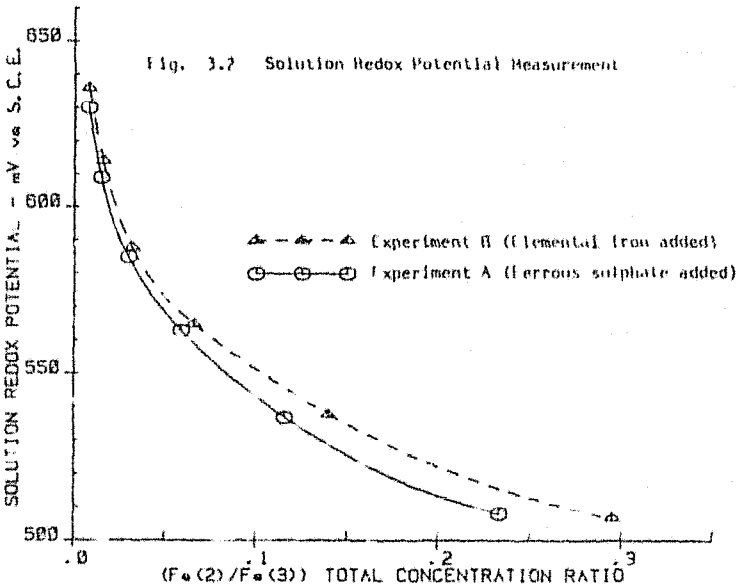


Fig. 3.2 Solution Redox Potential Measurement

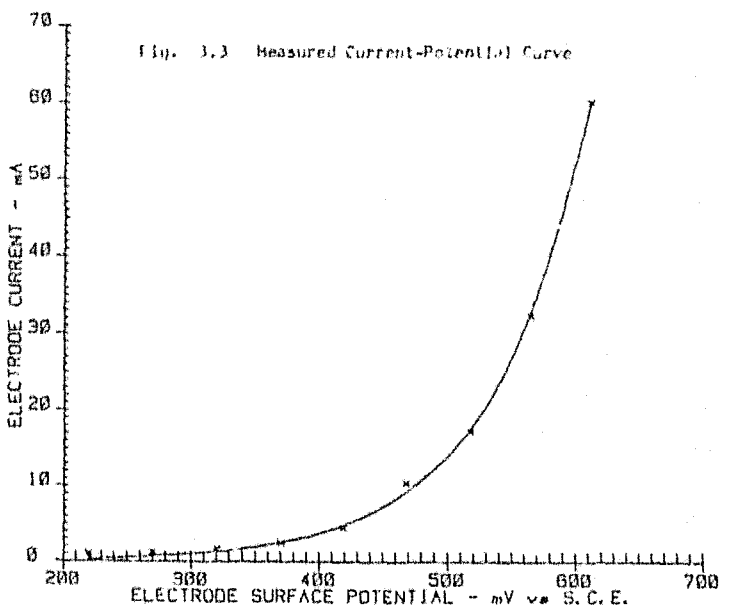


Fig. 3.3 Measured Current-Potential Curve

The curves obtained for copper and cobalt are similar to those for nickel and iron.

Figure 3.1(e) and (f) shows the potentials recorded during leaches 7 and 8, using a platinum (redox), a matte and a leached residue electrode (as described in section 2.2.2). In leach 7 the matte electrode was new, and leach 8 used the same matte electrode a second time. The residue electrode was used only once, for leach 8. The redox, matte and residue electrode potentials were all measured against the saturated calomel reference electrode. The potentials are all in millivolts.

3.2 Measurement of solution redox potential

Figure 3.2 summarises the results of the experiments done at 90°C to measure the solution redox potential as a function of total ferrous and ferric iron concentrations in the solution. In experiment A, ferrous ions were supplied by the addition of solid ferrous sulphate to the solution, thus keeping a constant ferric concentration. In experiment B, the ratio of ferrous to ferric iron was changed by the addition of powdered elemental iron, thus raising the ferrous and lowering the ferric concentrations by the following reaction:

$$2Fe^{3+} + Fe^{0} \rightarrow 3Fe^{2+}$$

Thus the total sulphate concentration remained constant during experiment B.

Tabulated results of these two experiments are given in Appendix III, along with the results of the measurements done at 22°C.

3.3 Electrochemical measurement of the matte leaching rate as a function of potential

The results of the measurement of the steady-state current-potential curve of a matte electrode are tabulated in Appendix IV, and summarised in Figure 3.3.

In Figure 3.3 the symbols represent experimental data points, and the solid line represents a function of the form:

$$i = A \exp(b E)$$

A, b = constants

The electrode surface potential was calculated by:

$$E = V - i R$$

Where: V = measured millivolts
i = measured milliamps
R = electrode resistance = 0,15Ω

The values of the constants A and B were found to be:

$$A = 0{,}019 \text{ mA}$$
$$B = 0{,}013 \text{ mV}^{-1}$$

3.4 Deportment of sulphur

a) Mineralogy

A sample of leach residue from leach 7 (90°C) was analysed by X-ray diffraction. The residue was found to contain elemental sulphur, magnetite and troilite. Plate III is a photomicrograph of the residue. The black rounded shapes are orthorhombic sulphur. The white particle inside a sulphur particle is troilite. Small grains of troilite, with a mean diameter of about 15 microns, occurred in some of the sulphur particles. These grains were clearly visible but were mostly occluded by the sulphur. From plate III, the interface between the elemental sulphur and the troilite seems to be clearly defined.

b) Sulphur analysis

Samples of fresh matte and leach residue from leach 9 (52°C) were analysed for total sulphur. The leach residue was also analysed for elemental sulphur. The results were as follows (mass %)

	Total S	Elemental S
Fresh matte :	30,4%	
Leach residue :	39,8%	13,4%

A sulphur balance over leach 9 can be calculated using the fresh matte and leach residue iron and total sulphur assays. The iron analyses were:

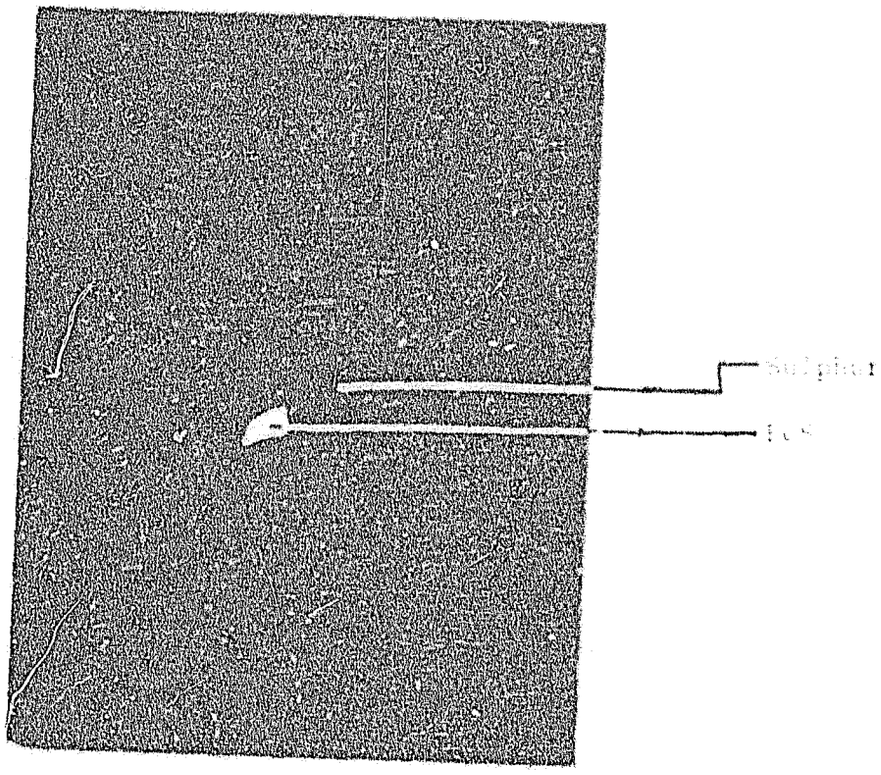


PLATE III: Photomicrograph of leach residue

The grain of FeS shown here has a diameter of about 20 - 30 microns

Fresh matte : 59,3% (mass)
Leach residue : 49,7% (mass).

The overall iron extraction was 44,4%. Therefore, assuming an initial amount of matte of 10 grams gives:

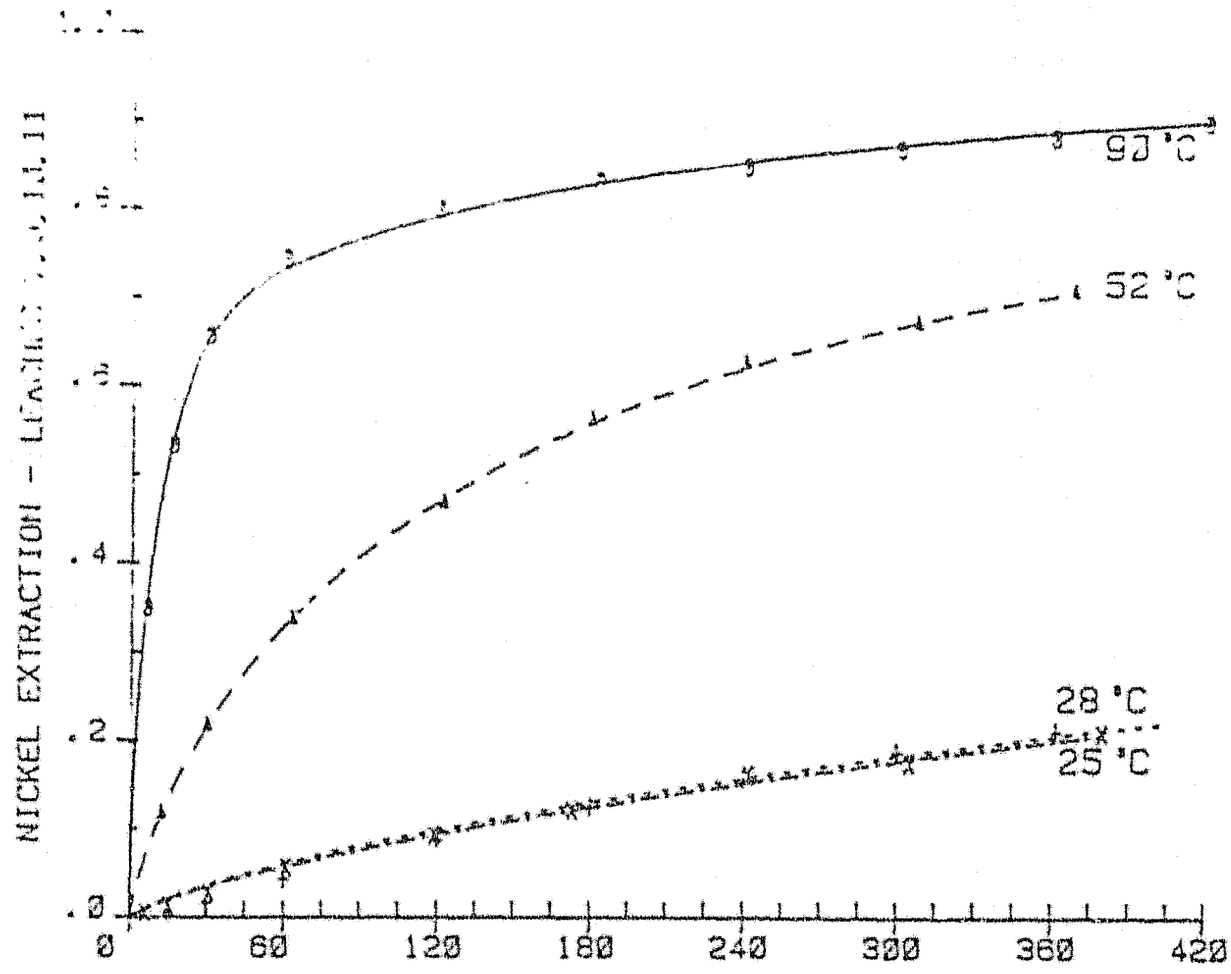
Total iron into leach	:	10.0,593	= 5,93 grams
Therefore iron remaining in residue:		5,93(1 - 0,444)	= 3,30 grams
Therefore mass of leach residue	:	3,30/0,497	= 6,63 grams
Total sulphur into leach	:	10.0,304	= 3,04 grams
Total sulphur ex leach	:	6,63.0,398	= 2,64 grams
Therefore sulphur lost during leach:		3,04-2,64	= 0,40 grams
Elemental sulphur ex leach	:	6.63·0,134	= 0,89 grams

Thus the percentage of reacted sulphur converted to elemental sulphur is :

$$\% S^{=} \rightarrow S^{o} = 100.0,89/(089 + 0,4)$$
$$= 69\%$$

3.5 Effect of temperature on leaching rates

Figure 3.4 shows the extraction vs time curves obtained for leaches 7 (90°C), 9 (52°C), 11 (28°C) and 10 (25°C). The cobalt and copper leaching curves are similar. As the leaching temperature decreased from 90°C, there was a dramatic decrease in the leaching rates.



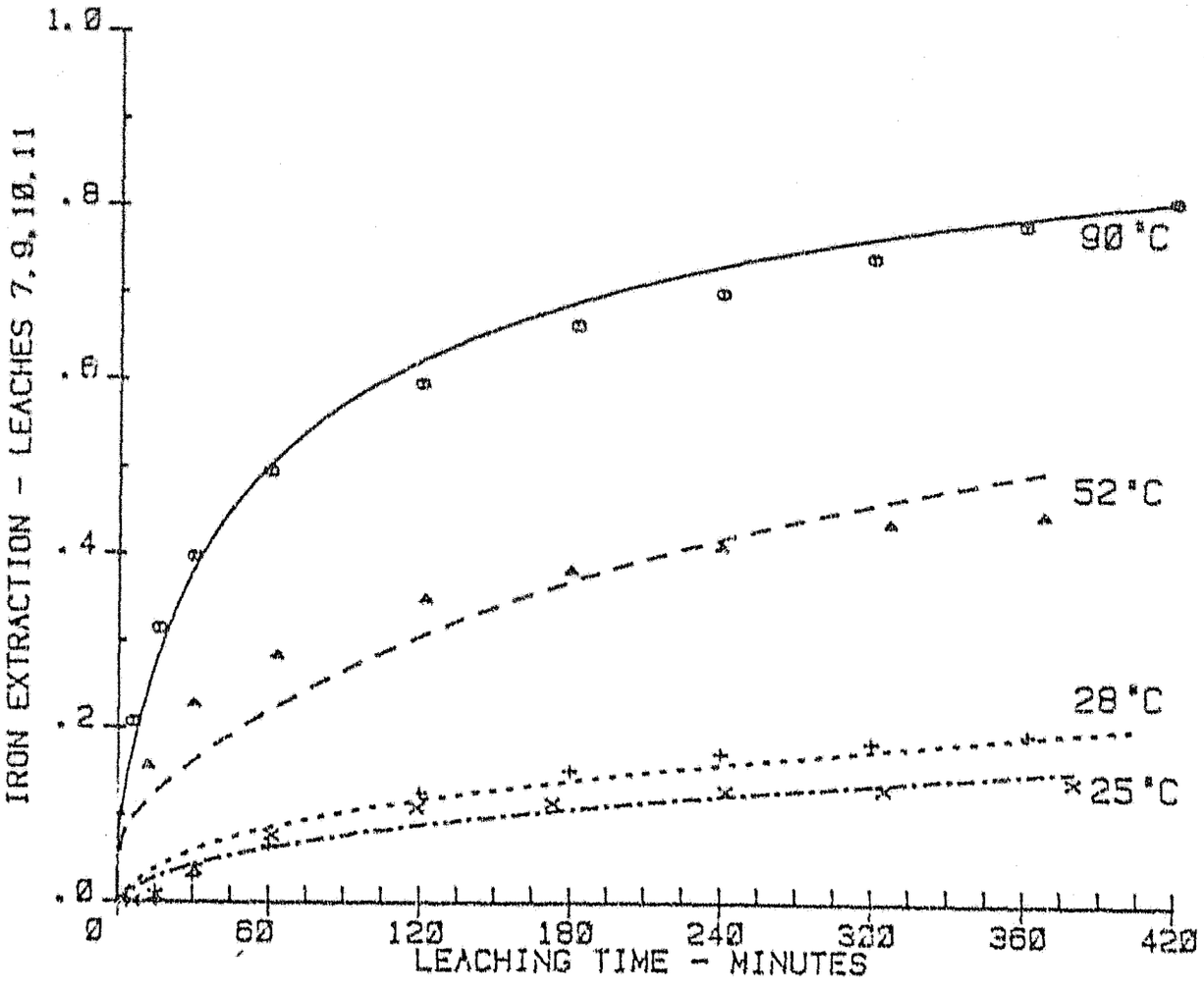


Fig. 3.4 Effect of temperature on leaching rates

4. THEORETICAL MODELLING OF THE EXPERIMENTAL RESULTS

4.1 Leaching of matte

Levenspiel(39) describes a good engineering model as one which gives the closest representation of reality without excessive mathematical complexity. The mathematical model used to describe the leaching results presented in this thesis must account for two aspects of the leaching, namely the behaviour of the reactants during leaching and the nature of the reaction between the leaching solution and the solid particles.

a) Behaviour of the solids during leaching:

Levenspiel(39) presents two idealised models for the noncatalytic reaction of particles with a surrounding fluid. These are the "progressive conversion" and the "unreacted core" models. The "progressive conversion" model assumes that the fluid enters and reacts throughout the particle at all times, not necessarily at a uniform rate throughout the particle. This means that solid reactant is converted throughout the particle, and that there is no interface between the reactant and any reaction products. For the "unreacted core" model, the assumption is made that reaction occurs first at the outer skin of the particle. The reaction zone then moves into the solid, leaving behind any solid reaction products and inert material. In this model there is a sharp interface between the solid reactant and any solid reaction products, and a core of unreacted material which shrinks in size as the reaction proceeds. In the "unreacted core" model, the rate of reaction may be controlled by diffusion of fluid reactants or products to or from the reacting interface, or by the reaction at the interface. In the case of diffusion control, the rate may be controlled either by diffusion through a reaction product layer, or by diffusion to or from the bulk fluid.

A variation of the above "unreacted core" model is the "shrinking particle" model, which is the same as the "unreacted core" (or "shrinking core") model, except that any reaction products formed do not form a layer around the unreacted solids - instead, they either flake off the main particle, or are formed as fluid

products, which then form part of the bulk fluid. In the case of chemical reaction at the reaction interface being the rate limiting step, the "shrinking particle" and the "shrinking core" models are mathematically identical.

In section 3 (experimental results), plate III shows a photomicrograph of leached residue particles. There is a clearly defined interface between the unreacted material and the solid reaction product, thus the "shrinking particle" or the "shrinking core" models described above would seem to be the most reasonable description of the solids behaviour during leaching. Figure 3.4 of section 3 shows that the affect of temperature on the leaching rates is large, thus the assumption can be made that the rates are controlled by chemical reaction and not by any form of diffusion, and therefore the "shrinking core" and "shrinking particle" models are mathematically identical in this case. The assumption of chemical reaction as the rate-controlling step will be further verified in section 5 of this thesis.

b) Leaching reactions:

The proposed stoichiometry of the leaching reaction is:

i) $MS + Fe_2(SO_4)_3 \rightarrow MSO_4 + 2FeSO_4 + S^o$

ii) $M^o + Fe_2(SO_4)_3 \rightarrow MSO_4 + 2FeSO_4$

M = Ni, Cu, Co or Fe in the sulphide or metallic phase.

Reaction (i) above is the same as that given by Lowe(3) for pyrrhotite, and fits the experimental results, in that elemental sulphur was observed in the leach residue, and ferric ions were reduced to ferrous ions during leaching.

A different stoiciometry for the leaching reactions could be:

iii) $MS + H_2SO_4 \rightarrow MSO_4 + H_2S$

iv) $M + H_2SO_4 \rightarrow MSO_4 + H_2$

v) $H_2S + Fe_2(SO_4)_2 \rightarrow H_2SO_4 + 2FeSO_4 + S^o$

vi) $H_2 + Fe_2(SO_4)_2 \rightarrow H_2SO_4 + 2FeSO_4$

This reaction scheme is much less plausible than reactions (i) and (ii) above. Nicol(40) presented experimental results for the non-oxidative dissolution of FeS. As the mineral surface potential went from -0,3 volts (*vs* the saturated calomel electrode) to more positive values, the reaction: $FeS + 2H^+ + 2e^- \rightarrow H_2S$ (reaction 6 in reference 40, with x = 0), decreased rapidly in rate. The open-circuit non-oxidative dissolution of the iron sulphide was also found to be strongly potential dependant, with the presence of oxidising agents strongly reducing the dissolution rate.

The leaching reported on in this thesis was done in strong ferric sulphate (oxidising) solution, at potentials much more positive than those used by Nicol. In view of this, reaction (iii) above does not seem plausible.

The reaction: $2H^+ + 2e^- \rightarrow H_2$ has a standard reduction potential of zero(18), thus at potentials negative to zero volts (*vs* standard hydrogen electrode) the above reaction will proceed as shown. At potentials positive to zero, the reaction would proceed in the reverse direction (if dissolved hydrogen were present in solution). In the leaching experiments done in this work, the matte electrode potential was always higher than +0,4 volts *vs* the saturated calomel electrode, thus higher than +0,6 volts *vs* the standard hydrogen electrode. Therefore reaction (iv) above is extremely improbable, and if no H_2S or H_2 is generated, equations (v) and (vi) cannot occur.

(c) Deportment of sulphur:

According to Krishnasivamy and Feurstenau(41), the general experience in oxidative leaching of sulphide minerals is that elemental sulphur does form, and resists oxidation at potentials below 0,8 volts *vs* the standard hydrogen electrode. Thermodynamically, though, elemental sulphur is a non-equilibrium species, the sulphate ion being the thermodynamically stable reaction product. The production of elemental sulphur instead of sulphate is due to slow sulphate-formation kinetics (42).

In the leaches done for this thesis, the solution redox potential (used to approximate the sulphide surface potential) were above 0,8 volts (*vs* standard hydrogen electrode) for the first few minutes of

leaching, and were close to 0,8 volts for the rest of the time. (See Figure 3.1(e) and (f) - 550 millivolts *vs* S.C.E. is approximately 0,79 volts *vs* standard hydrogen electrode). Thus one may expect elemental sulphur to form, and also to be at least partially oxidised to sulphate. If one assumes the rate-limiting step in the anodic dissolution of FeS to be (1,2) $S^{=} \rightarrow S^{o} + e^{-}$, and that the elemental sulphur so formed does not result in a rate-limiting diffusion barrier, then the subsequent partial oxidation of the elemental sulphur to sulphate must be assumed to have no effect on the rate of dissolution of the FeS. The assumption that the elemental sulphur does not give rise to a rate-limiting diffusion boundary will be re-examined in section 5.

d) Galvanic interactions:

The alloy phase in the matte was found to be in intimate contact with the troilite phase, but not all of the troilite phase was associated with alloy. Dobos(18) lists the following standard reduction potentials of electrochemical reactions (at 25°C):

i)	$FeS + 2e^{-} \rightarrow Fe + S^{=}$	$E^{o} = -1,01$ volts
ii)	$Fe^{2+} + 2e^{-} \rightarrow Fe$	$E^{o} = -0,441$ volts
iii)	$S^{o} + 2e^{-} \rightarrow S^{=}$	$E^{o} = -0,508$ volts
iv)	$Ni^{2+} + 2e^{-} \rightarrow Ni$	$E^{o} = -0,250$ volts

Adding equations (ii) and (iii) and subtracting equation (i) (along with the various E^{o} values), gives:

v)	$Fe^{2+} + S^{o} + 2e^{-} \rightarrow FeS$	$E^{o} = 0,06$ volts

This means that, at potentials negative to 0,06 volts, reaction (v) will proceed as written, from left to right. At potentials positive to 0,06 volts, the reaction will proceed in the reverse direction, i.e. FeS decomposing to give Fe^{2+} and S^{o} plus electrons.

According to equations (ii) and (iv), metallic nickel will decompose to Ni^{2+} at potentials positive to -0,25 volts, and metallic iron will decompose to Fe^{2+} at potentials positive to -0,441 volts, relative to the standard hydrogen electrode.

The major sulphide phase in the matte is troilite (FeS), and the alloy consists mainly of nickel and iron. Because the standard

reduction potentials of metallic nickel and iron are appreciably more negative than that of FeS, one may expect that, when a particle containing alloy and troilite is placed in an oxidising environment (i.e. a ferric sulphate solution), galvanic interaction between the metal and the FeS will inhibit the dissolution of the FeS, until all the metallic phase has dissolved. Obviously, if the particle does not contain any of the alloy phase, this will not occur, and the FeS will begin dissolving as soon as it is placed in the oxidising solution.

Now, in section 2.1.4 it was calculated that at least 88 per cent of the sulphide phase in the matte was not associated with alloy phase. This means that inhibition of FeS dissolution by galvanic interaction with alloy can only affect about 12 per cent of the matte, which greatly reduces its effect on the overall FeS leaching rate. Consider two equally large particles, one containing an alloy inclusion, the other containing only FeS. Let these two particles be placed simultaneously into an oxidising solution. In the particle containing only FeS, the FeS will immediately begin to dissolve. In the other particle, the FeS will not dissolve until all the alloy has dissolved. If, however, the rate of alloy dissolution is much faster than the rate of FeS dissolution, by the time that all the alloy has dissolved, only a small part of the FeS in the other particle will have dissolved. Now consider ten equally sized particles, only one of which contains an alloy inclusion. By the same reasoning as above, the effect of galvanic interaction in the alloy-containing particle on the overall dissolution of the FeS will be an order of magnitude smaller than for the alloy-bearing particle alone.

The above reasoning implies that, in the case of the matte under investigation, even though the alloy phase is not fully liberated from the troilite phase, the effects of galvanic interaction between the alloy and the troilite should be small. This assumption simplifies the mathematical model needed to explain the leaching results, and will thus be accepted at this stage. In section 5 (Application of the theory to the experimental results) this assumption will be re-examined in greater detail.

Obviously, in a different matte containing more alloy phase, the assumption of negligible galvanic effects may not be valid. However, where it is valid, this assumption allows the different phases in the

matte to be treated independently of one another, since all the phases can be regarded as leaching simultaneously, each phase at its own rate.

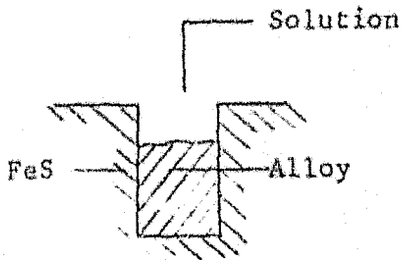
e) Effect of multiphase particles on the mineral surface area:

While a single phase troilite particle can be expected to show simple shrinking core behaviour during leaching, a particle of troilite, containing an alloy inclusion, may not do so. Galvanic interaction will prevent dissolution of the troilite until all the alloy has dissolved, leaving a cavity in the troilite. This cavity may so change the geometry that troilite leaching proceeds from within, as well as on the outer surface of the particle. This would result in leaching behaviour significantly different from that of the simple shrinking core model. However, it was calculated previously (see sub.section (c) above) that the effect of galvanic interaction should be small. Therefore the effect of multiphase particles on the overall mineral surface behaviour during leaching should also be small, because most of the troilite in the matte is not associated with alloy.

f) Behaviour during leaching of alloy surface area:

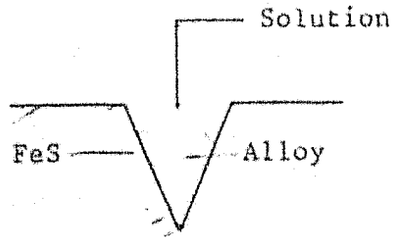
It can be seen from plates I and II in section 2 that, in the alloy-troilite particles, there is no obvious shape that can be considered representative of the alloy particles. Consider the following two idealised inclusion shapes:

i) Cylindrical



If the alloy inclusion were in the form of a cylinder, as shown above, the surface area exposed to the leaching solution would remain constant. Thus, assuming constant solution composition and surface reaction rate control, the leaching rate would be independant of the amount of alloy leached from the inclusion.

ii) Conical



If the inclusion were in the form of a cone, radius of base = r, height = h, then the following would apply:

The surface area of the base : $A = \pi r^2$

The volume of the cone : $\upsilon = (\pi/3)r^2h$

The base radius and the height of the cone are related by:

$$r/h = \mathrm{Tan}(\theta/2)$$

Thus : $h = r/\mathrm{Tan}(\theta/2)$

Therefore volume: $\upsilon = (\pi/3)r^3/\mathrm{Tan}(\theta/2)$

Therefore : $\upsilon = \alpha r^3$

$$[\alpha = (\pi/3)/\mathrm{Tan}(\theta/2)]$$

Therefore : $r = (\upsilon/\alpha)^{1/3}$

Thus, the surface area of the base of the cone is related to the cone volume as follows:

$$A = \pi r^2$$

Therefore : $A = \pi(\upsilon/\alpha)^{2/3}$

Therefore : $A = \alpha'\upsilon^{2/3}$

$$[\alpha' = \pi/\alpha^{2/3}]$$

Therefore, if the rate of leaching is proportional to the exposed surface:

$$\frac{dm}{dt} = -KA$$

K = some rate constant

m = metal in alloy phase

Then: $\frac{dm}{dt} = -K\alpha'\upsilon^{2/3}$

In the case of a conical alloy inclusion, then the rate of leaching of alloy, assuming constant solution conditions and surface reaction rate

control, depends on the amount of unleached alloy, raised to the power of 2/3.

In the actual matte, the alloy inclusions have complex shapes, thus theoretical prediction of the behaviour of the alloy surface area during leaching is not feasible. The area (and thus the leaching rate) could depend on the amount of alloy remaining unleached, or it could be independent of the extent of leaching. This aspect, too, will be re-examined in section 5.

4.1.1 Derivation of the model

The matte has been fully characterised in section 2.1. It consists of an iron-nickel alloy, troilite (FeS), magnetite (Fe_3O_4), and a copper, iron sulphide phase. These phases can be expected to leach at different rates. Also, there is a range of particle size present in the matte, thus there are different sized particles of the various phases present. Two different sized particles of the same phase can also be expected to leach at different rates. The model used to explain the leaching results should therefore take the different minerals present into account, as well as the particle size distribution.

The model used will first be derived for a single particle, then expanded to include the particle size distribution and the different minerals present.

4.1.1.1 Mineral surface behaviour

Consider a single particle of one mineral phase, leaching in the ferric sulphate solution. Assume that the rate of leaching of a metal (nickel, copper, cobalt, or iron) M from this particle, is directly proportional to the particle surface area.

Thus, the rate of change of the amount of nickel, copper, cobalt or iron left in the particle is given by:

$$\frac{dm}{dt} = -K\psi a \qquad (1)$$

Where: m = amount of metal left in the particle, g-moles

a = particle surface area, cm^2

K = rate constant, $g\text{-}mol \cdot cm^{-2} \cdot s^{-1}$

ψ = a factor accounting for the effect of solution conditions on the leaching rate, dimensionless.

The effect of the solution conditions will be dealt with further on.

At any given time, the particle will have a certain volume, given by:

$$\upsilon = \frac{m}{\rho^*} \qquad (2)$$

Where: υ = particle volume, cm^3

m = amount of the given metal in the particle, g-moles

ρ^* = molar density of the given metal in the particle, $g\text{-moles}\cdot cm^{-3}$

A characteristic particle size can be defined for the particle as:

$$d^3 = \upsilon \qquad (3)$$

Where: d = particle size, cm

υ = particle volume, cm^3

The surface area of the particle will then be:

$$a = \gamma d^2 \qquad (4)$$

Where: a = particle surface area, cm^2

d = particle size

γ = some shape factor.

Assume that the shape factor, γ, remains constant as leaching proceeds. This will be so if the particle shape (e.g., spherical) does not change.

Combining equations (3) and (4) gives:

$$a = \gamma \upsilon^{2/3}$$

Substituting for υ from equation (2) gives:

$$a = \gamma \left\{ \frac{m}{\rho^*} \right\}^{2/3}$$

Substituting this result into equation (1) gives:

$$\frac{dm}{dt} = -K\psi\gamma \left\{ \frac{m}{\rho^*} \right\}^{2/3} \qquad (5)$$

If the particle is leaching at the surface only, the molar density of the metal of interest will be constant during leaching, i.e.:

$$\rho^* = m_o/d_o^3$$

Where: m_o : value of m at time = zero
d_o : value of d at time = zero

Therefore, substituting for ρ^* in equation (5) gives:

$$\frac{dm}{dt} = - K\psi\gamma \, (d_o^3/m_o)^{2/3} \, (m)^{2/3} \qquad (6)$$

All the factors on the right hand side of equation (6) are constant, except for the solution conditions factor ψ and the amount of the metal m in the particle. Thus, if the variation of the factor ψ with time were known, equation (6) could be integrated to give the amount of metal m remaining in the particle, as a function of time. The model represented by equation (6) is simply the well-known shrinking core reaction model, with no diffusion resistance terms.

To expand this model towards the actual leaching situation, consider a large number n of particles, all of the same mineral and the same particle size, all leaching. In this case, the differential mass balance becomes:

$$\frac{d(nm)}{dt} = - nK\psi\gamma \, (d_o^3/m_o)^{2/3} \, (m)^{2/3} \qquad (7)$$

(i.e., multiply both sides of equation (6) by n)

Where: m = amount of metal m in a single particle, g-moles
n = total number of particles

Rearranging equation (7) gives:

$$\frac{d(nm)}{dt} = - K\psi\gamma \, (d_o^3/m_o)^{2/3} (n)^{1/3} \, (nm)^{2/3} \qquad (7a)$$

The number of particles, n, is given by:

$$n = F_o^*/(\rho \upsilon_o) = F_o^*/(\rho d_o^3) \quad (9)$$

Where: F_o^* = total initial mass of particles, g
ρ = mass density of particles, g cm^{-3}
υ_o = initial volume of a single particle, cm^3
d_o = initial particle size, cm

The amount of metal m in a single particle at time zero is:

$$m_o = M_o^*/n = M_o^* \rho d_o^3/F_o^* \quad (10)$$

Where: M_o^* : total moles of metal m in all the particles at time = 0, g-moles

Therefore, from equation (10):

$$m_o/d_o^3 = M_o^* \rho/F_o^* \quad (11)$$

Substituting from equations (9) and (11) into equation (7a) and rearranging gives:

$$\frac{d(nm)}{dt} = - K\psi\gamma \, F_o^*/(\rho d_o) \, (nm/M_o^*)^{2/3}$$

Dividing both sides by the reactor volume gives the rate of leaching per unit volume:

$$\frac{1}{V}\frac{d(nm)}{dt} = -K\psi\gamma \, F_o^*/(V\rho d_o) \, (nm/M_o^*)^{2/3} \quad (12)$$

Equation (12) represents the simple shrinking particle model, expanded to account for a large number of identical particles.

To expand the model again, this time to include different particles leaching simultaneously, consider a leach vessel of volume V, into which a total mass F of matte is poured. The particle size distribution of the matte is known, as well as the phase compositions of the different particle sizes present.

The mass of particles of a given particle size is then:

$$F_o' = \alpha F_o$$

Where: F_o' = total initial mass of particles of a given size, grams

F_o = total initial mass of all particles, grams

α = known fraction

Of the particles of a given size, a known fraction can be considered to comprise a given mineral, thus

$$F_o^* = \beta F_o' = \alpha \beta F_o \qquad (13)$$

Where: F_o^* = initial mass of particles of a given size, of a given mineral, grams

β = known fraction

Since the matte has been fully characterised, the initial amount of metal m in each mineral of each size fraction, is also known.

Therefore, the rate of leaching of all the particles of a given size and a given mineral, is found by substituting from equation (13) into equation (12):

$$\frac{1}{V}\frac{d(nm)}{dt} = -K\psi\gamma F_o \alpha\beta/(V\rho d_o)(nm/M_o^*)^{2/3} \qquad (14)$$

All the terms in equation (14) are known constants, except for the variable (nm) and the solution effect factor ψ. If the variation of ψ with time were known, equation (14) could be integrated to yield the variation with time of (nm).

Before evaluating the solution effect factor ψ, let us expand the model again, this time to include different minerals and different particle sizes. Consider again the leach vessel, into which F_o grams of matte are poured. The total leaching rate of a given metal will be the sum of all the individual leaching rates of the metal from the various minerals and particle sizes present, i.e.:

$$\frac{1}{V}\frac{d}{dt}\sum (nm)_{ij} = \sum\left\{\frac{1}{V}\frac{d(nm)_{ij}}{dt}\right\} \qquad (15)$$

Where: $(nm)_{ij}$ = amount of metal m in all the particles present of initial size d_{oi} of mineral j

i,j = indices denoting the different minerals and initial particle sizes present.

Equation (15) represents a set of uncoupled differential equations, which can be solved, once the variation of the solution effect factor, ψ, is known.

4.1.1.2 Effect of the leach solution

Brodie(1) and Paul, Nicol, Diggle and Saunders(2) found the anodic dissolution of lead sulphide to be electrochemical in nature, the basic process being:

$$PbS \rightarrow Pb^{2+} + S + 2e^{-}$$

Lowe(3) reported (page 100 of his thesis) that the leaching rates, per unit surface area for bornite, covellite and chalcopyrite are proportional to the exponential of the overpotential at the mineral surface, in ferric sulphate leaching.

Therefore, since the anodic dissolution of lead, copper and copper-iron sulphides has been shown to be electrochemical in nature, it would seem reasonable to assume that the anodic dissolution of iron sulphide, which constitutes the bulk of the matte used in this study, to be electrochemical in nature, as well. This assumption was experimentally substantiated. Details of this aspect are presented further on.

The basic relation used to describe electrochemical kinetics is the Butler-Volmer equation(4), which may be written as follows:

$$i = i_o \left[\exp\{(1 - \beta)Fn/(RT)\} - \exp\{ - \beta Fn / (RT)\}\right]$$

Where:
- i = current density
- i_o = exchange current density
- F = Faraday constant
- R = universal gas constant
- T = absolute temperature
- β = symmetry factor
- n = overpotential

The overpotential η, is the difference between the open-circuit potential of the electrode, and the potential when current is flowing, i.e.:

$$\eta = E - E_e$$

Where: E = potential with current flowing

E_e = open-circuit potential (no current)

Both these two potentials are measured against some reference electrode.

The complete Butler-Volmer equation contains anodic and cathodic reaction terms. In the case of anodic dissolution of iron sulphide, only the anodic term in the equation is of interest, thus the equation may be reduced to:

$$i = i_o \exp\{(1 - \beta)F(E - E_e)/(RT)\} \qquad (16)$$

The proposed overall anodic reaction for the dissolution of a metal sulphide is:

$$MS \rightarrow M^{2+} + S^o + 2e^-$$

Thus, the current at the electrode surface is related to the dissolution rate of the sulphide as follows:

$$-\frac{1}{a}\frac{dm}{dt} = 2Fi \qquad (17)$$

Where: a = electrode surface area

m = moles of metal sulphide

Substituting for i from equation (16) gives:

$$-\frac{1}{a}\frac{dm}{dt} = 2Fi_o\exp\{(1 - \beta)F(E - E_e)/(RT)\} \qquad (18)$$

For a given reaction, the symmetry factor β is a constant, thus, at constant temperature:

$$(1 - \beta)F/(RT) = \text{a constant}$$

For a given reaction system, i.e., a given sulphide and a given solution, the equilibrium potential, E_e and the exchange current density, i_o, will be constant at constant temperature. Therefore, equation (18) reduces under these conditions to:

$$-\frac{dm}{dt} = a\,K\exp\{kE\} \qquad (19)$$

Where: $K = 2Fi_o \exp\{- kE_e\}$ = constant

$k = (1 - \beta)F/(RT)$ = constant

Now, recall equations (1) and (6) from the previous sub-section:

$$\frac{dm}{dt} = - k\psi a \qquad (1)$$

$$\frac{dm}{dt} = -K\psi\gamma(d_o^3/m_o)^{2/3} (\bar{m})^{2/3} \qquad (6)$$

Dividing equation (6) by equation (1) and rearranging gives:

$$a = \gamma(d_o^3/m_o)^{2/3} (m)^{2/3} \qquad (20)$$

Where: a = particle surface area

γ = shape factor

m_o = initial amount of metal m present in the particle

$\bar{m}$ = amount of metal m in particle

Substituting equation (20) into equation (19) gives:

$$\frac{dm}{dt} = - K\gamma \left[\exp(kE)\right](d_o^3/m_o)^{2/3} (m)^{2/3} \qquad (21)$$

Equation (21) is identical to equation (6), with the solution effect factor ψ as

$$\psi = \exp(kE) \qquad (22)$$

Where: E = mineral surface potential

k = constant

Equations (14), (15) and (22) can be used to explain the leaching behaviour of the matte.

In summary, therefore, the leaching model assumes simple shrinking core behaviour of individual particles, and electrochemical reaction behaviour at the mineral surfaces. Different minerals will have different values of the constants K and k in the above set of equations.

4.1.1.3 Prediction of the dependence of the leaching rate of FeS on the mineral surface potential

Paul, Nicol, Diggle and Saunders(2) deduced the following mechanism for the anodic dissolution of galena (PbS):

$$\text{Step 1 :} \quad PbS \rightleftharpoons Pb^{2+} + S^{-} + e^{-}$$
$$\text{Step 2 :} \quad S^{-} \rightarrow S^{o} + e^{-}$$
$$\text{Overall:} \quad PbS \rightarrow Pb^{2+} + S^{o} + 2e^{-}$$

In the absence of information to the contrary, it would seem reasonable to assume that the anodic dissolution of troilite (FeS) proceeds in a similar fashion, i.e.:

$$\text{Step 1 :} \quad FeS \rightleftharpoons Fe^{2+} + S^{-} + e^{-}$$
$$\text{Step 2 :} \quad S^{-} \rightarrow S^{o} + e^{-}$$
$$\text{Overall:} \quad FeS \rightarrow Fe^{2+} + S^{o} + 2e^{-}$$

Although the derivation of the current-potential expression for this mechanism is exactly analogous to that of Paul *et al.*(2) for galena, it is presented here for the sake of completeness.

In deriving the current-potential curve, the assumption is made that the intermediate product (S^{-}) is at some steady state value, therefore:

$$\frac{d}{dt}[S^{-}] = 0 = \vec{i}_1 - \overleftarrow{i}_1 - \vec{i}_2 \qquad (23)$$

Where $\vec{i}_1$ and $\overleftarrow{i}_1$ are the anodic and cathodic currents for step 1, and $\vec{i}_2$ is the anodic current due to step 2.

Current-potential curves for the individual steps in the reaction mechanism can be calculated(4) as:

$$\vec{i}_1 = \vec{k}_1 F \exp\{(1 - \beta_1)FE/(RT)\} \qquad (23a)$$
$$\overleftarrow{i}_1 = \overleftarrow{k}_1 F [Fe^{2+}] [S^{-}] \exp\{-\beta_1 FE/RT)\} \qquad (23b)$$
$$\vec{i}_2 = \vec{k}_2 F [S^{-}] \exp\{(1 - \beta_2)FE/(RT)\} \qquad (23c)$$

Where: $[\ ]$: concentration in solution
$\vec{k}_1$: anodic rate constant for step 1
$\overleftarrow{k}_1$: cathodic rate constant for step 1

$\overleftarrow{k_2}$: anodic rate constant for step 2

β_1 : symmetry factor for step 1

β_2 : symmetry factor for step 2

F : Faraday constant

R : universal gas constant

T : absolute temperature

E : mineral surface potential

Rewriting equation (23) in terms of equations (23a), (23b) and (23c) rearranging gives:

$$[S^-] = \frac{\overrightarrow{k_1} \exp\{(1-\beta_1)FE/(RT)\}}{\overrightarrow{k_1}[Fe^{2+}] \exp\{-\beta_2 FE/(RT)\} + \overleftarrow{k_2} \exp\{(1-\beta_2)FE/(RT)\}} \quad (24)$$

The total anodic current is twice the current due to step 2, i.e.:

$$i_a = 2i_2$$

Therefore:

$$i_a = 2F\overleftarrow{k_2}[S^-] \exp\{(1-\beta_2)FE/(RT)\} \quad (25)$$

Substituting for $[S^-]$ from equation (24) gives:

$$i_a = \frac{2F\overrightarrow{k_1}\overleftarrow{k_2} \exp\{(2-\beta_1-\beta_2)FE/(RT)\}}{\overrightarrow{k_1}[Fe^{2+}] \exp\{-\beta_2 FE/(RT)\} + \overleftarrow{k_2} \exp\{(1-\beta_2)FE/(RT)\}}$$

This equation can be simplified further by assuming $\beta_1 = \beta_2 = 0,5$ (reference 4, page 918), and rearranging gives:

$$i_a = \frac{K^* \exp\{FE/(RT)\}}{[Fe^{2+}] \exp\{-FE/(2RT)\} + k^* \exp\{FE/(2RT)\}}$$

Where: $K^* = 2F\overrightarrow{k_1}\overleftarrow{k_2}/\overrightarrow{k_1}$

$k^* = \overleftarrow{k_2}/\overrightarrow{k_1}$

If the mineral surface potential is high enough, the first term in the denominator becomes small, and can be ignored, giving:

$$i_a = K^*/k^* \exp\{FE/(2RT)\}$$

$\overleftarrow{k}_2$: anodic rate constant for step 2

β_1 : symmetry factor for step 1

β_2 : symmetry factor for step 2

F : Faraday constant

R : universal gas constant

T : absolute temperature

E : mineral surface potential

Rewriting equation (23) in terms of equations (23a), (23b) and (23c) rearranging gives:

$$[S^-] = \frac{\overrightarrow{k}_1 \exp\{(1-\beta_1)FE/(RT)\}}{\overrightarrow{k}_1[Fe^{2+}] \exp\{-\beta_2 FE/(RT)\} + \overleftarrow{k}_2 \exp\{(1-\beta_2)FE/(RT)\}} \quad (24)$$

The total anodic current is twice the current due to step 2, i.e.:

$$i_a = 2i_2$$

Therefore:

$$i_a = 2F\overleftarrow{k}_2[S^-] \exp\{(1-\beta_2)FE/(RT)\} \quad (25)$$

Substituting for $[S^-]$ from equation (24) gives:

$$i_a = \frac{2F\overrightarrow{k}_1\overleftarrow{k}_2 \exp\{(2-\beta_1-\beta_2)FE/(RT)\}}{\overrightarrow{k}_1[Fe^{2+}] \exp\{-\beta_2 FE/(RT)\} + \overleftarrow{k}_2 \exp\{(1-\beta_2)FE/(RT)\}}$$

This equation can be simplified further by assuming $\beta_1 = \beta_2 = 0,5$ (reference 4, page 918), and rearranging gives:

$$i_a = \frac{K^* \exp\{FE/(RT)\}}{[Fe^{2+}] \exp\{-FE/(2RT)\} + k^* \exp\{FE/(2RT)\}}$$

Where: $K^* = 2F\overrightarrow{k}_1\overleftarrow{k}_2/\overrightarrow{k}_1$

$k^* = \overleftarrow{k}_2/\overrightarrow{k}_1$

If the mineral surface potential is high enough, the first term in the denominator becomes small, and can be ignored, giving:

$$i_a = K^*/k^* \exp\{FE/(2RT)\}$$

Thus, the anodic current, and therefore the dissolution rate of the FeS, can be expressed as:

$$i_a = K \exp\{k \cdot E\}$$

Where: $K = K^*/k^* \cdot$ = constant

$k = F/(2RT)$

$= 0{,}016\ mV^{-1}$ at 90°C (26)

If the anodic dissolution of FeS proceeds in the manner proposed above, the value of the constant k in the leaching model developed in section 4.1.1.2, for the troilite, should be given by equation (26).

4.1.1.4 Prediction of the dependence of the leaching rate of the alloy phase on the mineral surface potential

The alloy phase in the matte consists of about 40 per cent nickel and 60 per cent iron. Since this alloy contains a significant amount of nickel, it is possible that its leaching behaviour could be that of pure iron, pure nickel, or some intermediate. Detailed electrochemical experiments, which are outside the scope of this work, would be required to explain fully the behaviour of this alloy. Taking this into account, however, the behaviour of pure iron and pure nickel can be tried as possible approximations to the alloy leaching behaviour.

a) Iron

At anodic potentials above 580 mV (vs normal hydrogen electrode, i.e. above about 340 mV vs the saturated calomel electrode), the anodic dissolution of iron virtually stops, due to the formation of a passive surface layer(13). If the alloy leaching behaviour can be approximated by that of pure iron, the rate of leaching of the alloy should be independent of potential, because the leaching experiments were done at potentials above 400 mV vs S.C.E., and thus well into the passivation region of the iron.

b) Nickel

Both nickel(15) and iron - 10 per cent nickel alloy(16) form passive surface layers during anodic dissolution. Bartlett(17) gives an expression for the current in a passive layer as:

$$i_a = A \exp\{B\ E\}$$

Where E is the electric field across the layer, i is the current, and A and B are constants. This form of expression is the same as that used in the leaching model but no theoretical prediction of the values of the constants A and B can be made.

4.2 Solution redox potential

In order to use equation (22) of the previous section to predict the matte leaching rate, the value of the mineral surface potential must be known or approximated. Since the leaching solution was composed mainly of ferric and ferrous ions in sulphate solution, a convenient approximation of the mineral surface potential is the solution redox potential, as defined by the redox reaction:

$$Fe^{3+} + e^- \rightleftarrows Fe^{2+}$$

The use of the redox potential to approximate the mineral surface potential is justified in section 5.1.

4.2.1 The Nernst equation

The redox potential of the above ferric-ferrous couple is given by the Nernst equation, as follows:

$$E = E^o - \frac{RT}{F} \ln\left\{\frac{(Fe^{2+})}{(Fe^{3+})}\right\}$$

Where: E = solution redox potential

E^o = solution redox potential when Fe^{2+} and Fe^{3+} are at unit activity

R = universal gas constant

T = absolute temperature

F = Faraday constant

( ) = activity in solution

The problem with the Nernst equation, especially at higher electrolyte concentrations, is that the activity of any given species in solution need not be related to its concentration in a simple way. If the ferrous/ferric activity ratio in any given solution were known, the Nernst equation could be used to predict the solution redox potential. A number of assumptions can be made, in order to predict the ferrous/ferric activity ratio. The validity of these assumptions is examined in section 5.2.

a) Activity ratio equals total concentration ratio

The most obvious approximation of the ferrous/ferric activity ratio is simply the total ferrous/ferric concentration ratio in the solution. The reasoning for this approximation is that, no matter how complex the relation between an individual species activity and concentration may be, this relation may be similar for various species in solution. This suggests that the ratio between two species activities may be similar to the total concentration ratio between the two species. If this is so, then the total ferrous/ferric concentration ratio, when used in the Nernst equation, will result in the correct prediction of the solution redox potential.

b) Activity ratio proportional to total concentration ratio

If the ferrous/ferric activity and total concentration ratio differ by some constant factor, the Nernst equation can still be used, with the following modification:

$$E = E^{o} - \frac{RT}{F} \ln(\{Fe^{2+}\}/\{Fe^{3+}\})$$

Assume: $\{Fe^{2+}\}/\{Fe^{3+}\} = a[Fe^{2+}]/[Fe^{3+}]$

Where : $\{\ \}$ = activity

$[\ ]$ = concentration

a = constant factor

The Nernst equation then becomes:

$$E = E^{o} - \frac{RT}{F} \ln(a[Fe^{2+}]/[Fe^{3+}])$$

or $$E = E^{o} - \frac{RT}{F} \ln(a) - \frac{RT}{F} \ln([Fe^{2+}]/[Fe^{3+}])$$

This reduces to:

$$E = E' - \frac{RT}{F} \ln([Fe^{2+}]/[Fe^{3+}])$$

Where: $$E' = E^{o} - \frac{RT}{F} \ln(a)$$

Therefore, if the ferrous/ferric activity ratio is proportional (but not equal) to the total concentration ratio, the Nernst equation can still be used, but with a modified intercept (E' instead of E^{o}) which must be determined experimentally. The theoretical value of the slope is retained.

The above modified form of the Nernst equation will be called the "empirical" Nernst equation hereafter, because the value of the intercept (E') must be found empirically. When the correct ferrous/ferric normal potential (E^{o}) is used, the Nernst equation will be referred to as the "theoretical" Nernst equation.

(c) Activity ratio is proportional to some power of the total concentration ratio

The above assumption can be expressed mathematically as follows:

$$\{Fe^{2+}\}/\{Fe^{3+}\} = a([Fe^{2+}]/[Fe^{3+}])^{b}$$

Where: { } = activity
[ ] = concentration
a,b = constants

The Nernst equation then becomes:

$$E = E^{o} - \frac{RT}{F} \ln(a[Fe^{2+}]/[Fe^{3+}])^{b}$$

This reduces to:

$$E = A - B \ln([Fe^{2+}]/[Fe^{3+}])$$

Where: $A = E^{o} - B \ln(a)$
$B = bRT/F$

This form of the Nernst equation will be called the "best straight line" through the measured redox potential values, as a function of the total ferrous/ferric concentration ratio.

d) Activity ratio is related to the uncomplexed ferrous/ferric concentration ratio

A number of ferrous and ferric sulphate complexes have been reported in acid solution (5, 6). The nature of these complexes is discussed in section 4.2.2. Sapieszko *et al*(48) used the assumption that the solution redox potential can be predicted by the ratio of the uncomplexed ferrous/ferric concentrations and the "empirical" Nernst equation described in paragraph (b) above. Combination of the uncomplexed concentration ratio with the approximations in paragraphs (a), (b) and (c) above, results in three more estimates of the solution redox potential, i.e., the "theoretical" and "empirical" forms of the Nernst equation, and the "best straight line" of paragraph (c), all using the uncomplexed ferrous/ferric concentration ratio instead of the total ferrous/ferric concentration ratio. The mathematics for the calculation of the uncomplexed concentrations is given in Appendix V.

e) Use of individual Debye-Hückel activity coefficients

If the approximations in paragraphs (a) to (d) above prove inadequate, other ways must be sought to calculate the ferrous/ferric activity ratio. Using activity coefficients, the activity ratio between ferrous and ferric ions in solution is given by:

$$(Fe^{2+})/(Fe^{3+}) = \left\{\gamma_{Fe^{2+}}[Fe^{2+}]\right\} \Big/ \left\{\gamma_{Fe^{3+}}[Fe^{3+}]\right\}$$

Where: ( ) = activity
[ ] = concentration
γ = activity coefficient

The activity coefficient of an ionic species in solution is given by the Debye-Hückel equation (7) as:

$$-\log\gamma_i \qquad \frac{A\, z_i^2 \sqrt{I}}{1 + a_i B \sqrt{I}}$$

Where: γ_i = activity coefficient for species i

z_i = ionic charge of species i

a_i = ion size parameter of species i

A,B = constants characteristic of the solvent, (i.e. water) at the given temperature and pressure

I = ionic strength

Ionic strength is defined as:

$$I = \frac{1}{2} \sum c_i z_i^2$$

Where: c_i = concentration of species i

z_i = ionic charge of species i

Values for the parameter $\overset{o}{a}$ for the various species were taken from Oblad(6) and from Barner and Scheuerman(7). The values for the Debye-Hückel constants A and B were taken from Harned and Owen(8). The $\overset{o}{a}$ values used for the various species are listed in appendix VI.

Strictly speaking, the Debye-Hückel equation for activity coefficients is only valid at low ionic strengths(7). However, Morris (43) has found that when the formation of complex species is included in the calculations, the Debye-Hückel equation gives reasonable predictions of the mean activity coefficients of several divalent metal sulphates, up to ionic strengths of between 3 and 4. Willix(44) used an extended form of the Debye-Hückel equation to correlate the stability constant of the complex $FeSO_4^+$ as a function of ionic strength. He found fairly good agreement between the correlation and his experimental results, even though some of his results were at ionic strengths well above the region in which the use of this equation is strictly valid. At this stage, therefore, the assumption is made that the Debye-Hückel equation can be used at the ionic strengths (up to between 3 and 4) found in this work. This assumption will be re-examined in section 5.2.

By using the activity coefficients and the various complex equilibria, one can calculate the activities of the uncomplexed ferrous and ferric species in the leach solution. (The mathematics for this are given in Appendix V.) The activities of the uncomplexed ferric and ferrous ions can then be used in the Nernst equation to calculate

the solution redox potential. The value of the ferric/ferrous standard potential is given by Yeager and Salkind(93) as:

E^{o} = 0,771 volts at 25°C *vs* the standard hydrogen electrode

$\frac{dE^{o}}{dT}$ = 1,19 millivolts/K

In this work, the reference electrode used was a saturated calomel electrode (S.C.E.) which has a potential of 0,241 volts relative to the standard hydrogen electrode (S.H.E.) at 25°C (9). The standard potential of the ferric/ferrous redox reaction at 25°C, therefore, is:

E^{o} = 0,771 -0,241 = 0,530 volts *vs* S.C.E. at 25°C

The standard potential at temperatures other than 25°C is:

E^{o} = 771 + 1,19 (T - 298,15) mV *vs* S.H.E.

When using the S.C.E. in concentrated sulphate solution, the liquid junction potential between the K Cl electrolyte of the S.C.E. and the sulphate solution is not negligible, and must be included in the calculation of the measured solution redox potential. The Henderson equation(10) can be used to approximate this liquid junction potential:

$$\varepsilon_D = \frac{\sum\left\{(u_j/z_j)(c_{j,2} - c_{j,1})\right\}}{\sum\left\{u_j(c_{j,2} - c_{j,1})\right\}} \left\{\frac{RT}{F}\right\} \ln \frac{\sum\left\{u_j c_{j,2}\right\}}{\sum\left\{u_j c_{j,1}\right\}}$$

Where:
- ε_D = liquid junction potential
- u_j = ionic mobility of species j
- $c_{j,1}$ = concentration of species j in the K Cl electrolyte
- $c_{j,2}$ = concentration of species j in the sulphate solution
- F = Faraday constant
- R = universal gas constant
- T = absolute temperature at junction

Instead of ionic mobilities, limiting ionic conductivities can be used in the Henderson equation(10). Values for the limiting ionic conductivities were taken from Meites(11), and are given in Appendix VII. Values of limiting conductivity for the iron sulphate complex species were approximated by values for other ions of similar charge. This was done because examination of the values for several ionic species in Meites suggested that the main factor in determining the limiting conductance, is ionic charge.

The calculated value of the liquid junction potential must be added to the externally measured redox potential, to give the value calculated by the Nernst equation. Alternatively, the liquid junction potential can be subtracted from the Nernst equation redox potential, to give the externally measured value.

4.2.2 Complex species formed

a) Ferric species

The following ferric-complex equilibria have been reported in the literature:

i) $Fe^{3+} + SO_4^{=} \rightleftharpoons FeSO_4^{+}$

ii) $Fe^{3+} + HSO_4^{=} \rightleftharpoons FeHSO_4^{2+}$

iii) $Fe^{3+} + 2SO_4^{=} \rightleftharpoons Fe(SO_4)_2^{-}$

iv) $Fe^{3+} + HSO_4^{-} + SO_4^{=} \rightleftharpoons FeHSO_4SO_4$

Table 4.1 lists some of the reported stability constants for the above complex species. These values are concentration quotients, valid for the temperature and ionic strength indicated. If individual activities are to be used to calculate the solution redox potential (4.2.1c), it would seem logical to use individual activities in the calculation of the distribution of the various species in solution. This in turn requires the true thermodynamic equilibrium constants (i.e., at zero ionic strength) for the above reactions. Smith and Martell(47) critically reviewed the published information on a very large number of complex species. They gave values for the stability constants at zero ionic strength of the species $FeSO_4^{+}$ and $Fe(SO_4)_2^{-}$ at 25°C as follows:

Species	Stability constant
$FeSO_4^{+}$	8710 - 13 800
$Fe(SO_4)_2^{-}$	240 000

Sapieszko *et al*(48) found that, at low pH values, the major species present in acid ferric sulphate solution were uncomplexed Fe^{3+}, $FeSO_4^{+}$ and $FeHSO_4^{2+}$, at an ionic strength of 2,67. The total ferric and sulphate concentrations were 0,18 and 0,53 molar respectively. The concentration of $Fe(SO_4)_2^{-}$ was considered, but was discarded because it was consistently found to be negligibly small. This seems to contradict the findings of Whiteker and Davidson(90) and of Lister and Rivington(91). These authors found evidence for the formation of $Fe(SO_4)_2^{-}$ at much lower sulphate concentration - less than 0,1 molar - than was used by Sapieszko *et al*. The data given by Smith and Martell (47) for $Fe(SO_4)_2^{-}$ is much scantier than their data for $FeSO_4^{+}$. It would

TABLE 4.1

Ferric sulphate complexes : Some published data

Species	Temp, °C	Ionic strength	Stability constant	Source
$FeSO_4^+$	25	0	14100	Willix(44)
	18	0	15000	Sykes(89)
	19	0	7100	
	18	0,066	1040	
	19	0,066	525	
	19	0,15	228	
	25	0,5	205 ± 18	Davis and Smith(20)
	28	1,0	95	Whiteker and Davidson(90)
	25	2,67	84 ± 7	Sapieszko *et al*(48)
	25	5	210 ± 3	Ashurst and Hancock(49)
$FeHSO_4^{2+}$	19	0,15	60	Sykes(89)
	25	0,5	0 ± 1	Davis and Smith(20)
	25	1,2	6 ± 1	Lister and Rivington(91)
	25 - 80	2,67	4 ± 1	Sapieszko *et al*(48)
$Fe(SO_4)_2^-$	28	1,0	893	Whiteker and Davidson(90)
	25	1,2	16600	Lister and Rivington(91)
$FeHSO_4SO_4$	25	1,2	380 ± 50	Lister and Rivington(91)

seem, therefore, that there is disagreement in the literature over the stability of the complex $Fe(SO_4)_2^-$.

Table 4.1 shows only one discordant point in the stability data for $FeHSO_4^{2+}$, i.e., that of Davis and Smith(20). These authors studied the kinetics of formation of $FeSO_4^+$, and concluded that the formation quotient of $FeHSO_4^{2+}$ was less than one hundredth of that of $FeSO_4^+$ at an ionic strength of 0,5. However, they inferred that their experimental data was insufficient to permit conclusive determination of the $FeHSO_4^+$ stability constant, and therefore used their finding only to establish that the influence of $FeHSO_4^{2+}$ was small under their experimental conditions, thus allowing them to observe the formation of $FeSO_4^+$. Smith and Martell(47) give no data for $FeHSO_4^{2+}$. No value was found for this stability constant at zero ionic strength.

The complex $FeHSO_4SO_4$ was postulated by Lister and Rivington. No other authors have reported evidence for the existence of this species. In particular, Sapieszko *et al*(48) did not require this species in order to explain their results. It is possible, therefore, that $FeHSO_4SO_4$ is not a stable species in acid ferric sulphate solutions.

b) Bisulphate complex

Data on the stability of the bisulphate ion, HSO_4^-, has been extensively reported. Smith and Martell(47) give values for the stability constant and heat of formation at zero and several non-zero ionic strengths. Pitzer(22) presented a set of equations which represent the behaviour of pure sulphuric acid, including the formation of HSO_4^-.

c) Ferrous species

Various authors (6, 63, 92) have quoted values for the stability constants of $FeSO_4$ and $FeHSO_4^+$. It seems, however, that all these values, directly or indirectly, came from the work of Beukenkamp and Harrington(21). They used an ion-exchange technique to study the nature of the complexing between ferrous iron and sulphate in acid solution. The ionic strength in their experiments was not controlled. They gave the equilibrium constants for the formation of $FeSO_4$ and $FeHSO_4^+$ as

follows:

$$\frac{[FeHSO_4^+]}{[Fe^{2+}][HSO_4^-]} = 0,61$$

$$\frac{[FeSO_4]}{[Fe^{2+}][SO_4^{=}]} = 1,7$$

Where [ ] denotes concentration in solution

Smith and Martell(47) give the value for the stability constant of $FeSO_4$ (at 25°C and zero ionic strength) as 158, and the heat of formation as 6,7 kJ/mol. Wells and Salam(70) give values for the stability constants of $FeSO_4$ and $FeHSO_4^+$ as follows:

$$\frac{[FeSO_4]}{[Fe^{2+}][SO_4^{=}]} = 10 \text{ at } 25°C \text{ and ionic strength } 1$$

$$\frac{[FeHSO_4^+]}{[Fe^{2+}][HSO_4^-]} = 1,94 \text{ at } 25°C \text{ and ionic strength } 4$$

However, Wells and Salam give values at other temperatures for these stability constants which imply that they decrease with increasing temperature. In the case of $FeSO_4$, this is in conflict with the data given by other authors (47, 76), which indicates that these constants increase with increasing temperature. This seems to throw some doubt on the validity of Wells and Salam's approach (i.e., the measurement of the rate of reaction of Fe^{2+} with hydrogen peroxide) as regards determination of the stability constants of $FeSO_4$ and $FeHSO_4^+$. This implies that the work of Beukenkamp and Herrington(21) should be accepted, even though their ionic strength was not controlled. No other literature was found reporting these constants.

4.2.3 Estimation of stability constants at zero ionic strength

Values have been reported in the literature for the stability constants of $FeSO_4^+$, $Fe(SO_4)_2^-$, HSO_4^- and $FeSO_4$ at zero ionic strength. No values at zero ionic strength have been found for $FeHSO_4^{2+}$, $FeHSO_4^+$ and

$FeHSO_4SO_4$. Therefore these values must be estimated in some way.

One way in which estimates of the above stability constants can be made is by using individual Debye-Hückel activity coefficients at non-zero ionic strength to convert the stability constants at non-zero ionic strength to zero ionic strength. As an example, consider the stability constant of $FeSO_4^+$. At 25°C, the values of this stability constant at various ionic strengths are(47,48):

Ionic strength	Stability constant
0,5	138 - 219
1,0	83 - 132
2,67	77 - 91

Values of the individual Debye-Hückel activity coefficients at 25°C are as follows(6,7,8):

Species	Individual activity coefficient		
	I = 0,5	I = 1,0	I = 2,67
Fe^{3+}	0,0887	0,0689	0,0515
$SO_4^=$	0,1781	0,1308	0,0869
$FeSO_4^+$	0,7475	0,7231	0,6956

I = Ionic strength

Now, if K° is the stability constant of $FeSO_4^+$ at zero ionic strength, K is the value at some non-zero ionic strength, and $\alpha_{Fe^{3+}}$, $\alpha_{SO_4^=}$ and $\alpha_{FeSO_4^+}$ are the activity coefficients at the non-zero ionic strength, then:

$$K^\circ = \frac{\alpha_{FeSO_4^+}\left[FeSO_4^+\right]}{\alpha_{Fe^{3+}}\left[Fe^{3+}\right]\alpha_{SO_4^=}\left[SO_4^=\right]}$$

and:

$$K = \frac{\left[FeSO_4^+\right]}{\left[Fe^{3+}\right]\left[SO_4^=\right]}$$

Where [ ] denotes concentration.

Therefore : $K^\circ = \left\{ \frac{\alpha_{FeSO_4^+}}{\alpha_{Fe^{3+}}\alpha_{SO_4^=}} \right\} K$

Multiplying the stability constants at non-zero ionic strength by the above activity coefficient factor gives the following results for the stability constant at zero ionic strength:

Ionic strength for K	Calculated K°
0,5	6530 - 10400
1,0	6660 - 10600
2,67	12000 - 14100

The value of the stability constant of $FeSO_4^+$ is given by Smith and Martell(47) as being between 8710 and 13800 at zero ionic strength and 25°C. The values calculated via the individual ionic activity coefficients are surprisingly close to these reported values. Further justification for the use of individual Debye-Hückel activity coefficients is given in section 5.2. The calculation of values for the stability constants of $FeHSO_4^{2+}$, $FeHSO_4^+$ and $FeHSO_4SO_4$ by the above technique is shown in Appendix V. The values are as follows:

Reaction	Stability constant
$Fe^{3+} + H^+ + SO_4^= \rightleftarrows FeHSO_4^{2+}$	1900 - 4900
$Fe^{2+} + H^+ + SO_4^= \rightleftarrows FeHSO_4^+$	400
$Fe^{3+} + H^+ + 2SO_4^= \rightleftarrows FeHSO_4SO_4$	$6,9.10^6 - 9,3.10^6$

The stability constant of $FeHSO_4SO_4$ is based on only one report(91) and the possibility does exist (see section 4.2.2(a)) that this is not a stable complex, i.e., its stability constant may be very small.

4.2.4 Assumption implicit in the use of the Nernst equation

It is not impossible that at least some of the above complexes take part in electron exchange reactions(44). The Nernst equation, however, is only valid for a single redox couple. In order to use the Nernst equation to calculate the redox potential in ferric-ferrous sulphate solution, therefore, the assumption must be made that a single couple

(in this case Fe^{3+}/Fe^{2+}) dominates the redox reaction, and that any other redox reactions occurring (e.g. $FeSO_4^+ + e^- \rightleftarrows FeSO_4$) exert a negligible influence on the overall exchange current density, and therefore on the redox potential of the solution. If this assumption is not made, the Nernst equation cannot be used, and exchange current densities for all the exchange reactions are needed to calculate the solution equilibrium potential via the Butler-Volmer equation. Such data is simply not available in the literature for sulphate-complexed ferric and ferrous ions exchanging electrons at a platinum surface. Sapieszko *et al*(48) also used the assumption that the uncomplexed ferric/ferrous couple dominates the solution redox potential.

Although it is possible that the above assumption is erroneous, it is shown in section 5.2 that its use results in good agreement between predicted and measured values of the solution redox potential.

4.3 Electrochemical measurement of the matte leaching rate

The mathematical model proposed in section 4.1 for the matte leaching rate assumes the leaching reaction to be electrochemical in nature. An electrochemical reaction is described as a function of potential by the Butler-Volmer equation, which can be reduced, as shown in sub-section 4.1.1.2, to equation (19) of that sub-section:

$$-\frac{dm}{dt} = a\,K\,\exp\{k\,E\} \qquad (19)$$

The overall chemical dissolution reaction is:

$$MS \rightarrow M^{2+} + S^{o} + 2e^{-}$$

Where M: Ni, Cu, Co, or Fe

Thus the dissolution current is given by:

$$i = 2F\left\{\frac{-dm}{dt}\right\}$$

Thus: $i = 2F\,a\,K\,\exp\{k\,E\}$

Where: i = dissolution current
a = mineral surface area
F = Faraday constant
K,k = constants
E = mineral surface potential

The constants K and k are known from analysis of the leaching rate data, thus the currents due to dissolution of nickel, copper, cobalt and iron from the matte can be calculated, for a number of surface potentials. The sum of these currents gives an overall current-potential curve for the leaching of the matte, in which case the electrons generated are consumed by the reduction of ferric ions to ferrous ions at the matte surface. However, if the leaching reaction is electrochemical in nature, the method of removal of the electrons produced is irrelevant. If an electrode were made from the matte and placed in an inert solution (for example sodium sulphate), and then an anodic current were passed through this electrode, the electrode surface would assume a certain potential (relative to a reference electrode) at any given current density. In this case, the electrons are being removed from the electrode face by an external power source. Various currents can be passed, and a current-potential curve for the matte electrode in the inert electrolyte can be obtained. The form of this curve will be given by equation (19) above. If the value of the constant k in this equation agrees to within reasonable limits with the value of k obtained from the leaching experiments, it means that the effect of potential on the dissolution rate is independent of the means of production of the potential (i.e., of the means by which the electrons are removed from the matte surface), and therefore that the leaching of the matte is electrochemical in nature.

5. APPLICATION OF THE THEORY TO THE EXPERIMENTAL RESULTS

5.1 Leaching rate model

The mathematical model of the matte leaching rate consists of a set of differential equations. The leaching experimental results are in the form of fractional extraction of nickel, copper, cobalt and iron as functions of leaching time. In order to fit the model to the experimental results, the model must be integrated. This cannot be done explicitly, due to the exponential term containing the mineral surface potential, which varies with time. Therefore, the model must be integrated numerically. Accordingly, the model was written into a Fortran V computer programme, and solved using an Eclipse S250 computer. This programme is shown in Appendix VIII.

The computer programme uses the sum of the squared differences between the predicted and measured extractions (at the times of sampling) during the leach, to calculate the values of the constant K in equation 14 (section 4.1.1.1) for each element (Ni, Cu, Co or Fe) leaching from each mineral present. The values of the constant k (equation 22, section 4.1.1.2) were initially assigned values as detailed in section 4.1.1.3. These values were then modified by trial and error, in such a way as to reduce the total squared error (described above) as far as possible. At a given set of values for the constants k, the programme used the first and second partial derivatives of the total squared error with respect to the various constants K, to find the set of values for K that gave the minimum total squared error. When the total squared error is at a minimum, all the partial first derivatives must be zero (to suitable tolerance), and all the partial second derivatives must be positive.

Since the object of this work was to produce a mathematical model for the leaching of the matte, rather than a computer technique for the solution of this kind of problem, no mathematical proof of convergence for the computer solution of the model was attempted. The results of fitting the model to the experimental data show that the technique does work in this case.

5.1.1 Effect of different potentials on the fit of the leaching model

The leaching model was fitted to the experimental results of leaches 7 and 8. During these two leaches, the potentials of a platinum electrode, a matte electrode and a leached residue electrode were recorded against leaching time. These measured potentials were used to fit the model to the experimental data. Table 5.1 shows the resulting sums of squared differences between predicted and measured extractions of nickel, copper, cobalt and iron. Figure 5.1 shows the results of fitting the leaching model to the nickel extraction *vs* time data from leach 7, using the solution redox potential and the matte electrode potential to approximate the particle surface potential during leaching. Similar results were obtained for copper, cobalt and iron extractions in leach 7, and for nickel, copper, cobalt and iron extractions in leach 8. Graphs showing these results, and the leaching model computer printouts, are given in Appendix IX.

The results shown in Table 5.1 show that the best overall fit of the leaching model to the experimental data, was obtained when the redox potential was used to approximate the mineral surface potential during leaching. The next best fit resulted from the use of the residue electrode potential, followed by the partially leached matte electrode, while using the new matte electrode potential gave the worst fit of the model to the data. In the case of the nickel, copper and cobalt in leach 8, use of the residue electrode potential gave slightly better fits between the model and the data, but no great penalty was incurred by using the redox potential. In the case of the iron, use of the redox potential gave the best fit.

The better fit of the model to the experimental data obtained by using the solution redox potential instead of the new matte electrode potential to approximate the particle surface potential, can be explained in terms of the galvanic interactions mentioned in section 4.1(d), as follows:

TABLE 5.1

Effect of using redox, matte or residue electrode potentials as the particle surface potential during leaching, on the fit of the leaching model to the experimental results

Leach	Potential used	Sum of squared differences				
		Ni	Cu	Co	Fe	Total
7	Redox	0,0012	0,00023	0,0015	0,0019	0,0048
8	Redox	0,00044	0,0037	0,0037	0,0065	0,0143
7	Matte (1)	0,0054	0,018	0,00034	0,028	0,0517
8	Matte (2)	0,00050	0,0040	0,0010	0,018	0,0235
8	Residue	0,00036	0,0029	0,0010	0,012	0,0163

1) New matte electrode
2) Partially leached matte electrode

Note:
The results in this table were obtained by fitting the leaching model to leaches 7 and 8 separately.

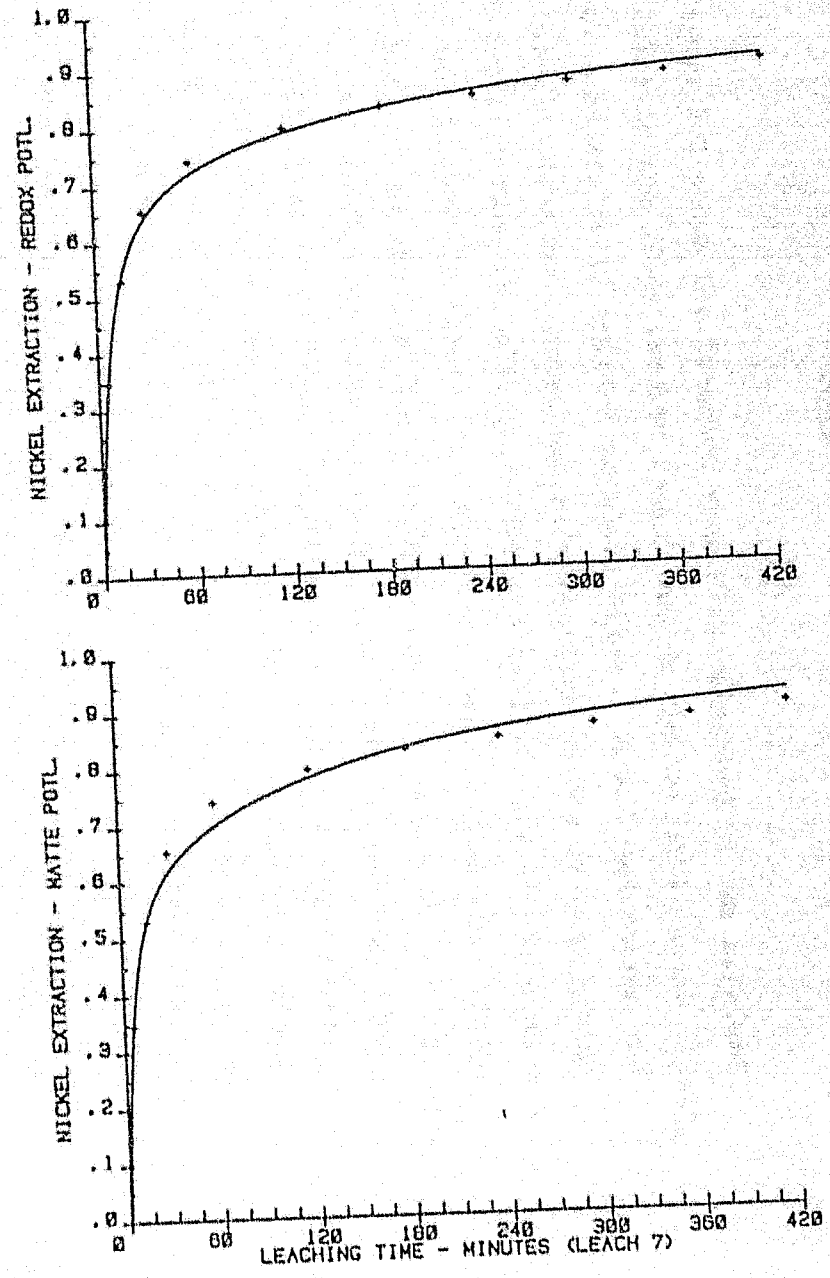


Fig. 5.1

TABLE 5.1

Effect of using redox, matte or residue electrode potentials as the particle surface potential during leaching, on the fit of the leaching model to the experimental results

Leach	Potential used	Sum of squared differences				
		Ni	Cu	Co	Fe	Total
7	Redox	0,0012	0,00023	0,0015	0,0019	0,0048
8	Redox	0,00044	0,0037	0,0037	0,0065	0,0143
7	Matte (1)	0,0054	0,018	0,00034	0,028	0,0517
8	Matte (2)	0,00050	0,0040	0,0010	0,018	0,0235
8	Residue	0,00036	0,0029	0,0010	0,012	0,0163

1) New matte electrode

2) Partially leached matte electrode

Note:
The results in this table were obtained by fitting the leaching model to leaches 7 and 8 separately.

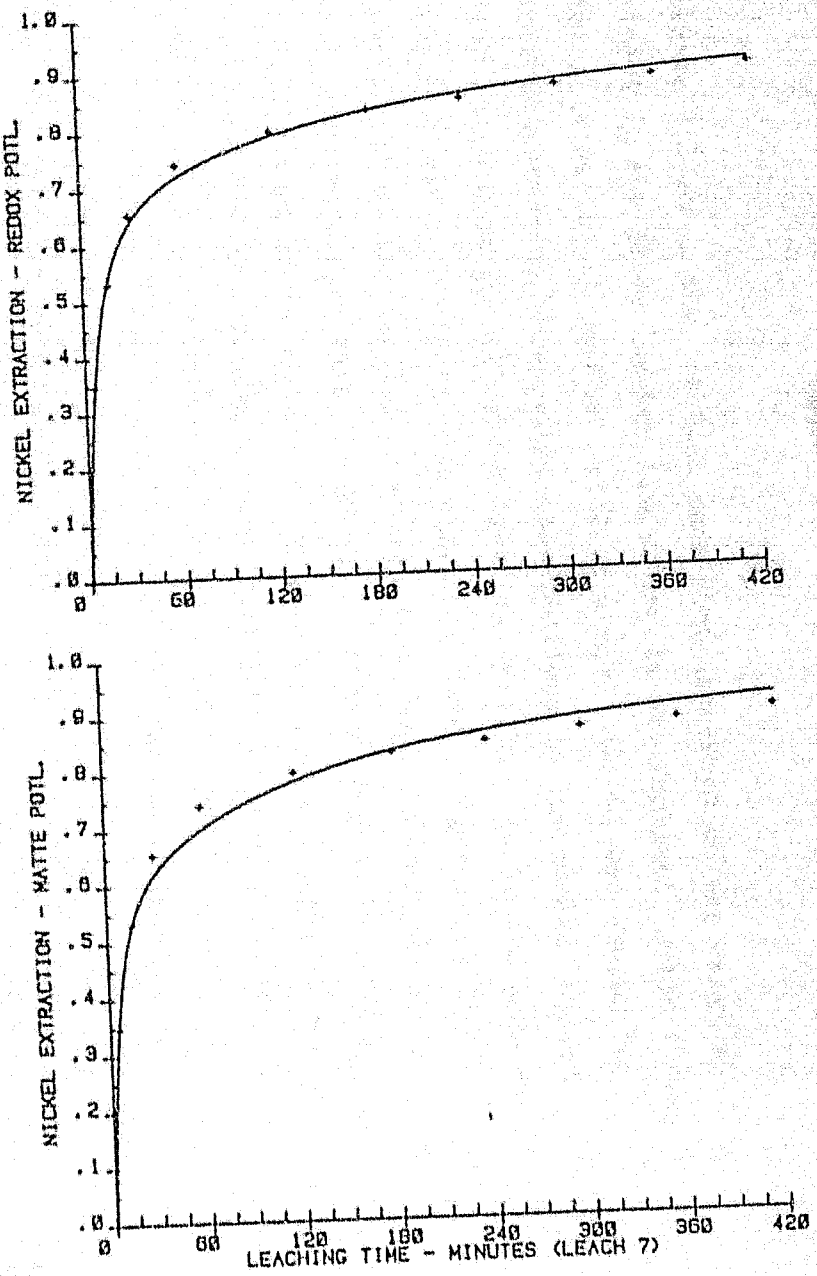


Fig. 5.1

Figure 5.2 shows the fraction remaining unleached of the original nickel in the alloy (broken lines) and in the troilite (solid lines), for a selection of initial particle sizes. Nickel was chosen for this illustration because the contributions to the overall nickel extraction from the alloy and from the troilite are of the same order of magnitude. In theory iron should be used, because this is the major part of the troilite - except that the contribution to the overall iron extraction from the alloy is so much smaller than from the troilite that it is virtually negligible. Therefore the nickel curves in Figure 5.2 are considered more likely to represent the actual amounts of unleached alloy and troilite at any given leaching time.

Table 5.2 lists, for all the initial particle sizes used, the time for complete dissolution of the alloy in any given particle size, and the fraction of troilite remaining unleached when the alloy has just all dissolved, both ignoring the allowing for the effect of galvanic interactions. The effect of galvanic interaction was calculated by assuming that, for any given particle size, the fraction of that particle size that contained alloy inclusions (section 2.1.4) did not leach at all while unleached alloy was present. The fraction of the troilite not associated with alloy leached as calculated by the leaching model. Thus, a particle of (initially) 73,9 microns was 93 per cent unleached after almost 2 hours of leaching, ignoring galvanic effects. In this size range, 24 per cent of the troilite was associated with alloy, thus when the effect of galvanic interaction is included, the amount unleached changes to:

$$1 - (1 - 0,93)(1 - 0,24) = 0,95$$

The effect of galvanic interactions is to reduce the amount of troilite leached from 7 per cent to 5 per cent for this size fraction. Table 5.2 shows that this is the maximum effect. The smaller particles are affected less, because they contained less alloy to start with. The particle size from 18,8 microns upwards represent the cyclosizer fraction 6, i.e., 46 per cent of the total matte, thus the error in the overall troilite dissolution due to ignoring galvanic interaction is, in this case, less than 1 per cent. This is within the experimental uncertainty of the leaching results.

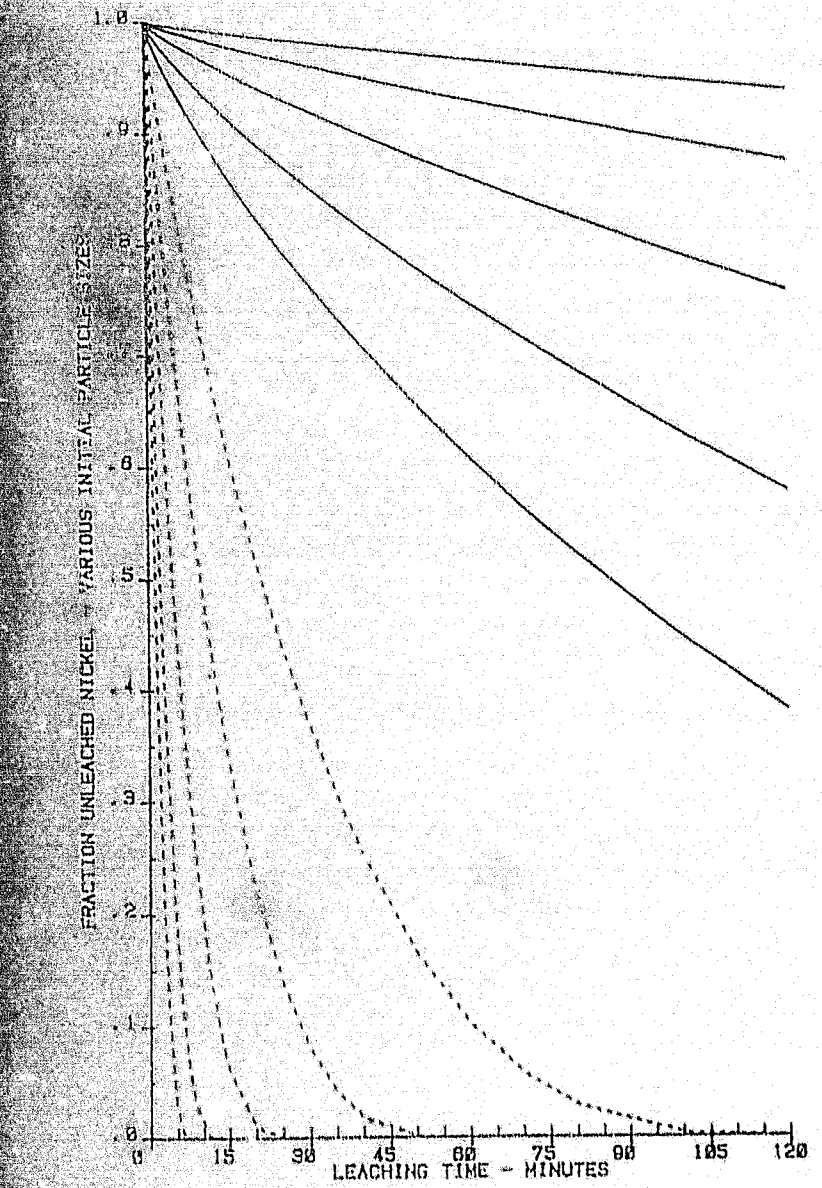


Fig. 5.2 Calculated fraction Ni in unleached particles

TABLE 5.2

Effect of neglecting galvanic interaction between alloy and troilite

Initial particle size, microns	Time for complete dissolution of alloy fraction, t = t*, min.	Fraction of troilite not yet leached at t = t*	
		Ignoring galvanic effects	Including (a) galvanic effects
2,4	2,2	0,91	0,91
3,3	3,4	0,91	0,91
4,6	4,7	0,91	0,91
5,7	5,0	0,92	0,92
7,1	7,4	0,92	0,92
10,1	8,6	0,92	0,92
13,9	12,9	0,92	0,92
18,8	18,1	0,93	0,95
20,1	25,2	0,93	0,95
36,9	37,8	0,93	0,95
52,2	55,5	0,93	0,95
73,9	80,5	0,93	0,95
105	118,5	0,94	0,95

(a) These figures were calculated using the assumption that the fraction of troilite associated with alloy does not dissolve at all until all the alloy has dissolved, while the rest of the troilite dissolves as before

In the case of the matte electrode, however, all of the troilite is in electrical contact with the alloy, and therefore galvanic interaction is not negligible in the matte electrode. The effect of galvanic interaction is to lower the electrode potential (while alloy is present) to a value lower than that of the bulk of the particles in the leach vessel. Figure 5.2 shows that almost 2 hours are needed to dissolve all the alloy from the leaching particles. At two hours the overall iron extraction is about 50 per cent for the particles, but due to galvanic interaction the iron extraction from the matte electrode must be small, only alloy having leached. This implies that the bulk of the leaching particles are at potentials greater than the potential of the matte electrode, which in turn suggests that the redox potential may be a better approximation of the particle surface potential than the matte electrode potential.

Figure 3.1(e) (section 3.1) shows that the potential of the matte electrode increased slowly until about 2 hours of leaching, then dropped again. The maximum at two hours is in agreement with the calculated time of two hours for total dissolution of the alloy (Figure 5.2).

In the case of the partially leached matte electrode the galvanic effect was not as strong as for the new matte electrode (Figure 3.1(f), leach 8). Even though the electrode was re-polished before leach 8, the amount of alloy at the face was probably much less than was originally the case. The shapes of the potential *vs* time curves for the residue and partially leached matte electrodes were much more similar to the redox potential curve than was the case for the new matte electrode.

Another explanation of the better fit of the leaching model to the experimental data when solution redox potential is used, which applies to the partially leached matte and residue electrodes, is as follows:

First, the assumption is made that the ferric/ferrous exchange current density at the surface of a leaching matte particle is large enough to make the effect of the anodic current due to the leaching of the matte negligible. Thus the matte surface potential will be equal to the redox potential of the solution at the matte surface. Now, as the matte dissolves, solid elemental sulphur is left behind.

This sulphur forms a layer through which the ferric ions must diffuse inwards, and the ferrous (and Ni^{2+}, Cu^{2+} and Co^{2+}) ions must diffuse outwards, as leaching progresses. This diffusion causes the concentrations of the ferrous and ferric ions at the matte surface to be different to those in the bulk solution, and therefore the redox potential at the matte surface to differ from that of the bulk solution.

The overall leaching reactions are:

a) Troilite leaching:

$$MS + Fe_2(SO_4)_3 \rightarrow M\,SO_4 + 2FeSO_4 + S^o$$

b) Alloy leaching:

$$M^o + Fe_2(SO_4)_3 \rightarrow M\,SO_4 + 2FeSO_4$$

M in the above reactions represents nickel, copper, cobalt or iron, and for the purposes of this discussion is taken as representing only iron, since iron is the bulk of the metal in the matte.

From the above equations, we see that for every mole of iron leached from the matte, two moles of ferric ions must diffuse to the matte surface, and three moles of ferrous ions must diffuse away. There is also a total flux of one mole per mole leached, away from the matte surface. The concentration differences across the sulphur layer can be approximated (ref. 18, page 15) as follows:

a) Ferric ions:

$$F = \frac{D}{\delta l}\{C_\infty - C_s\} - F^*$$

b) Ferrous ions:

$$F = \frac{D}{\delta l}\{C_s - C_\infty\} + F^*$$

Where:
- F = flux of ferric or ferrous ions
- F^* = net outward flux of ions
- D = diffusivity
- δl = thickness of sulphur layer
- C_∞ = bulk solution concentration
- C_s = concentration at matte surface

If the rate of leaching of metal from the matte is r, then the fluxes are as follows:

Ferric ions : $F = 2r$

Ferrous ions : $F = 3r$

Nett flux out : $F^* = r$

Substituting these values into the above equations gives:

For ferric ions:

$$C_s = C_\infty - \frac{3r\delta 1}{D}$$

For ferrous ions:

$$C_s = C_\infty + \frac{2r\delta 1}{D}$$

The value of the reaction rate r, as a function of leaching time, is known from the leaching model. The thickness of the sulphur layer can be estimated by assuming that as matte is leached away, the sulphur remains behind, occupying the same volume as the unleached matte. Since the density and composition of the matte are known, the volume occupied by a given number of moles of iron in the matte can be calculated. Since the elemental sulphur formed has been found to be orthorhombic sulphur, which has a density of 2,07 g cm^{-3}, and the matte density is about 4,8 g cm^{-3}, the voidage in the sulphur layer will be about 60 per cent. The only remaining properties needed are the diffusivities of ferric and ferrous ions. Madsen(45) measured the diffusivity of the ferric ion in sulphate solutions of various concentrations. From these measurements, the value of the ferric ion diffusivity at 90°C and 2,7 molar sulphate concentration (corresponding to 100 g/1 Fe^{3+} in sulphate solution), is $5,6 \cdot 10^{-6}$ $cm^2 s^{-1}$, or $3,3 \cdot 10^{-4}$ cm^2/minute. This is fairly close to the value given by Lowe(18) of $5 \cdot 10^{-4}$ cm^2/minute. Chapman(19) gives the diffusivity of copper and zinc ions in aqueous solution at 25°C as $3,8 \cdot 10^{-6}$ $cm^2 s^{-1}$ (at a concentration of 1,4 g moles l^{-1}) and $5,7 \cdot 10^{-6}$ $cm^2 s^{-1}$ (at 0,25 g moles l^{-1}) respectively. Since the copper and zinc diffusivities decrease with increasing concentration, and diffusivity increases with increasing temperature, the very rough approximation can be made that the diffusivity of ferrous iron in the leaching solution is the

same as the diffusivity of the copper, given above. The diffusivities found in this manner are by no means claimed to be accurate, but they should be at least of the correct order of magnitude. The above diffusion coefficients must be multiplied by the voidage fraction of the sulphur layer, to give values for the diffusivities in this layer. Thus, the diffusivities to be used are:

$$\text{Ferric}: \quad D = 2 \cdot 10^{-4} \text{ cm}^2 \text{ min}^{-1}$$

$$\text{Ferrous}: \quad D = 1{,}5 \cdot 10^{-4} \text{ cm}^2 \text{ min}^{-1}$$

Once the thickness of the sulphur layer is known, and the values have been estimated for the ferric and ferrous diffusivities, the change in concentrations across the sulphur layer can be calculated if the leaching rate is known. In the case of single matte particles, the leaching rate per cm^2 is given by the leaching model, as a function of potential. In the case of the matte electrode, one further complicating factor arises, i.e.:

Since the electrode was made by compressing matte particles together, and the face was ground using 1000 grit water paper, the electrode face cannot be considered to be smooth. The actual mineral surface area available for leaching is greater than the superficial surface area. A surface roughness factor can be defined as:

$$\text{S.R.F.} = \frac{\text{actual surface area}}{\text{superficial surface area}}$$

The leaching rate per cm^2 of electrode surface area is then given by the rate predicted by the leaching model, multiplied by the surface roughness factor. From the comparison between the electrochemically measured current potential curve and the curve predicted by the leaching model (next section), a value of 22 was deduced for the surface roughness factor.

The above method was used to calculate the surface concentrations of ferric and ferrous ions, and from these concentrations the solution redox potentials at the matte surface. This was done for the matte electrode, and for the largest initial matte particle size. The results of these calculations are shown on Figure 5.3. The symbols represent measured redox and matte electrode potentials, the solid line is calculated bulk solution redox potential, the dashed line is calculated redox potential at the matte electrode surface, and the dotted

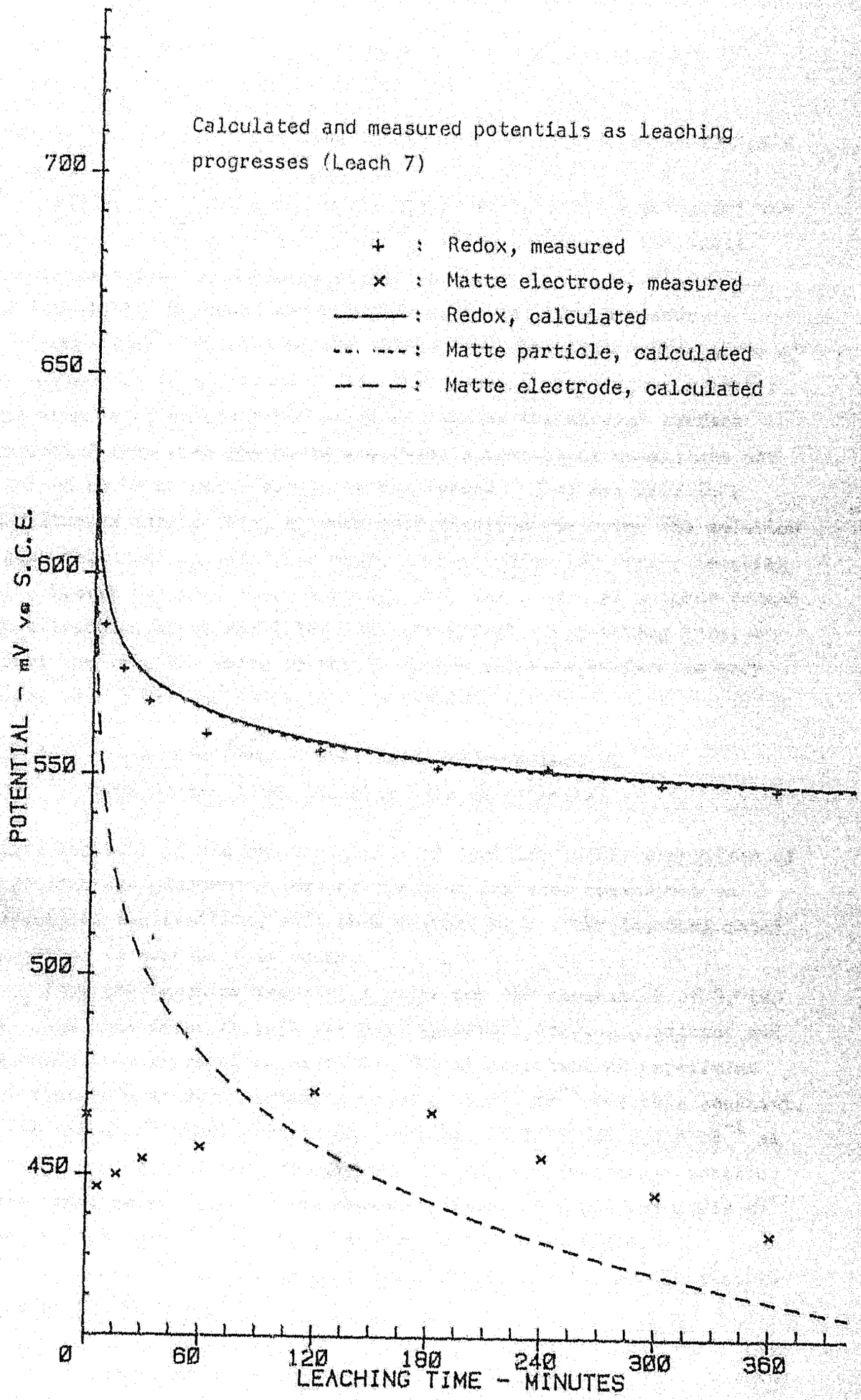

Calculated and measured potentials as leaching progresses (Leach 7)
+ : Redox, measured
× : Matte electrode, measured
——— : Redox, calculated
--- ---- : Matte particle, calculated
— — — : Matte electrode, calculated
POTENTIAL - mV vs S.C.E.
700
650
600
550
500
450
0
60
120
180
240
300
360
LEACHING TIME - MINUTES

Fig. 5.3

line is redox potential at the surface of the largest matte particle present.

Figure 5.3 shows that, while the particle surface potential remains very close to the bulk solution redox potential, the matte electrode potential deviates significantly from the solution redox potential, by an amount which increases as leaching proceeds.

Once again, it must be emphasised that these two explanations of an unexpected result (namely that the leaching model gives a better fit when solution redox potential is used as the mineral surface potential than when the matte electrode potential is used), are not claimed to be accurate models of the system. They are used in a qualitative manner only, as some justification for using the solution redox potential to model the matte surface potential during leaching.

Figure 5.3 does show, however, that the elemental sulphur formed on a leaching matte particles does not affect the leaching rate, because the solution redox potential at the sulphate surface is very close to the bulk solution redox potential.

5.1.2 Comparison between predicted and experimental dependence of the leaching rate on potential

Since the bulk of the matte consists of troilite (FeS), comparison of predicted and measured values of the leaching rate dependence on potential, for troilite, will show whether or not the leaching model developed in section 4 is sound.

From the leaching results, a value for the constant k of 0,019 mV^{-1} has been found to give the best agreement between predicted and measured iron extractions at 90°C. The electrochemical experiment (section 3.3) at 90°C yielded a value of 0,013 mV^{-1} for this constant, while the theoretical prediction (section 4.1.1.3) was 0,016 mV^{-1} at 90°C, assuming that the symmetry factors for the individual reaction steps were equal to 0,5. The measured values of 0,013 and 0,019 mV^{-1} can be used to calculate the symmetry factor β_1 as follows:

In section 3.1.1.3, the full rate expression for anodic dissolution of the FeS was:

$$i_a = \frac{2F\overleftarrow{k}_1\overleftarrow{k}_2 \exp\{(2-\beta_1-\beta_2)FE/(RT)\}}{\vec{k}_1[Fe^{2+}] \exp\{-\beta_2 FE/(RT)\} + \overleftarrow{k}_2 \exp\{(1-\beta_2)FE/RT\}}$$

At high potentials, this reduces to:

$$i_a = K^*/k^* \exp\{(1-\beta_1)FE/(RT)\}$$
$$= K \exp\{kE\}$$

The various symbols have the same meanings as in section 4.1.1.3.

Thus:

$$k = (1-\beta_1)F/(RT)$$

or: $k = (1-\beta_1)0,032$

The values for the symmetry factor β_1, as calculated from the leaching and electrochemical measurement results, for the leaching of iron from the troilite phase, are as follows:

From electrochemical measurement: $\beta_1 = 0,59$

From leaching results : $\beta_1 = 0,41$

Tamamushi(14) quotes anodic transfer coefficient (1-β) values for the reaction $Fe^{3+} + e^- \rightarrow Fe^{2+}$, on a platinum surface, which vary between 0,39 and 0,58. This means that the accuracy with which the symmetry factor for iron dissolution from troilite was determined from electrochemical and leaching measurements, is of the same order as the agreement between published values of the symmetry factor for the ferric-ferrous redox couple. The agreement between the electrochemical and leaching results is therefore acceptable, and the electrochemical leaching model assumed earlier is justified.

In summary therefore, the leaching mechanism of troilite in ferric sulphate solution can be considered to be electrochemical in nature. The mineral surface potential is best approximated by the solution redox potential, for the purposes of fitting the leaching model to the experimental data. The mineral surface potential may differ from the redox potential by a constant amount, without any detrimental effect on the fit of the model, since:

$$K \exp\{k(E - E^*)\} = K^* \exp\{k E\}$$

Where: $K^* = K \exp(-k E^*)$

$= $ constant if E^* is constant.

Thus the effect of any constant difference between the redox potential and the actual mineral surface potential is compensated for in the constant K in the leaching model.

5.2 Solution redox potential

The various equations and approximations discussed in section 4.2 were written into a Fortran V computer programme and solved on the Eclipse S250 computer. The computer printouts are shown in Appendix III.

5.2.1 Redox potential at ambient temperature

The effects of the various assumptions made regarding the ferrous/ferric activity ratio (section 4.2) were investigated using the measurements done at 22°C.

a) Total concentration ratio

Figure 5.4 shows the effect of using the total ferrous/ferric concentration ratio as an approximation of the ferrous/ferric activity ratio. The "theoretical" Nernst equation predictions are far from the measured values, while the "empirical" Nernst equation and the "best straight line" predictions are very similar, and give average and maximum differences between predicted and measured values of about 10 and 18 millivolts, respectively. This means that the "empirical" Nernst equation, with an intercept value of 682,7 millivolts, and the total ferrous/ferric concentration ratio, can be used to predict the redox potential with a maximum error of less than 20 millivolts. However, as is shown next, better predictions are possible.

b) Uncomplexed concentration ratio

The result of allowing for the complexes $FeSO_4^+$, HSO_4^- and $FeSO_4^o$, and using the uncomplexed ferrous/ferric concentration ratio to approximate the activity ratio, is shown in Figures 5.5 and 5.6. When the concentration quotients are taken from the literature, the results in Figure 5.5 are obtained, i.e., the "theoretical" Nernst equation gives

Where: $K^* = K \exp\{- k E^*\}$

$= \text{constant if } E^* \text{ is constant.}$

Thus the effect of any constant difference between the redox potential and the actual mineral surface potential is compensated for in the constant K in the leaching model.

5.2 Solution redox potential

The various equations and approximations discussed in section 4.2 were written into a Fortran V computer programme and solved on the Eclipse S250 computer. The computer printouts are shown in Appendix III.

5.2.1 Redox potential at ambient temperature

The effects of the various assumptions made regarding the ferrous/ferric activity ratio (section 4.2) were investigated using the measurements done at 22°C.

a) Total concentration ratio

Figure 5.4 shows the effect of using the total ferrous/ferric concentration ratio as an approximation of the ferrous/ferric activity ratio. The "theoretical" Nernst equation predictions are far from the measured values, while the "empirical" Nernst equation and the "best straight line" predictions are very similar, and give average and maximum differences between predicted and measured values of about 10 and 18 millivolts, respectively. This means that the "empirical" Nernst equation, with an intercept value of 682,7 millivolts, and the total ferrous/ferric concentration ratio, can be used to predict the redox potential with a maximum error of less than 20 millivolts. However, as is shown next, better predictions are possible.

b) Uncomplexed concentration ratio

The result of allowing for the complexes $FeSO_4^+$, HSO_4^- and $FeSO_4^o$, and using the uncomplexed ferrous/ferric concentration ratio to approximate the activity ratio, is shown in Figures 5.5 and 5.6. When the concentration quotients are taken from the literature, the results in Figure 5.5 are obtained, i.e., the "theoretical" Nernst equation gives

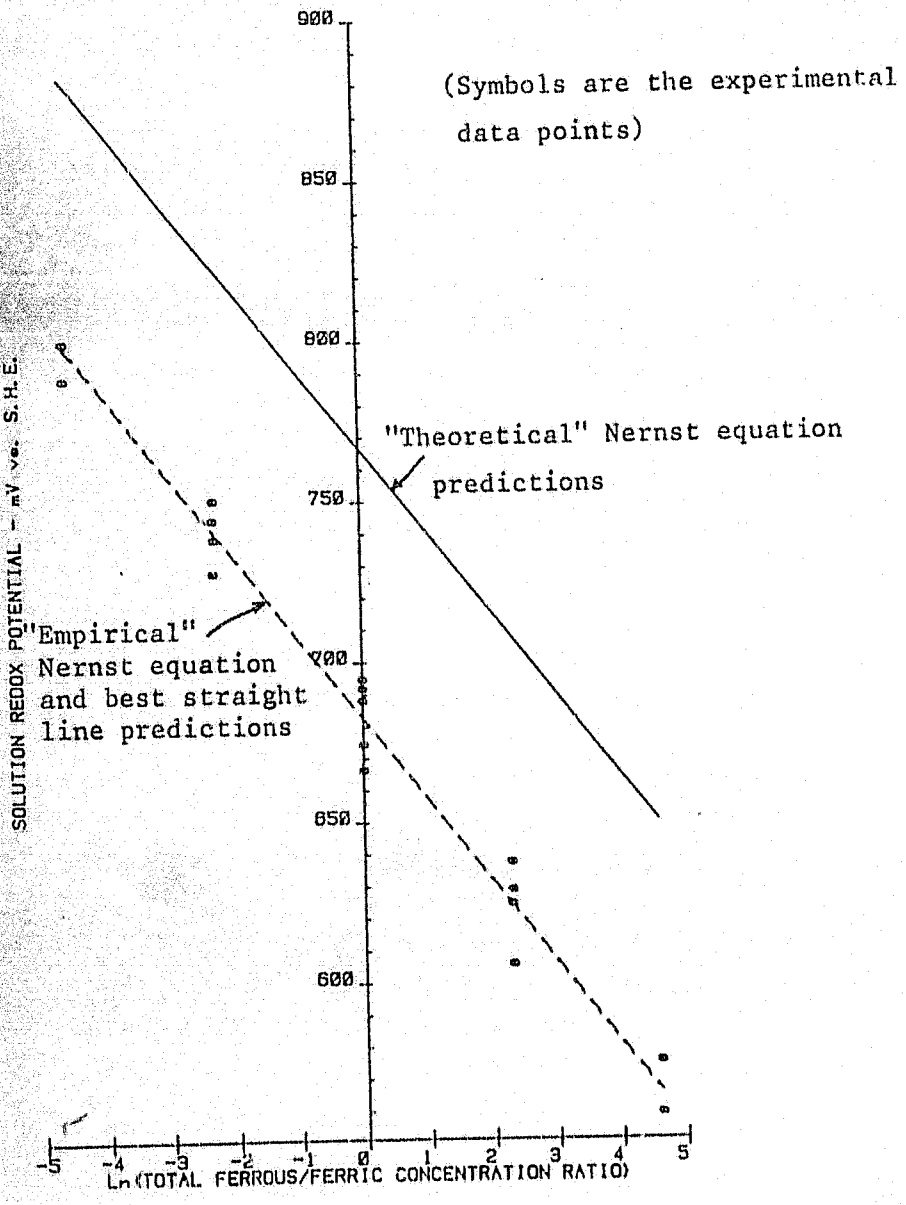

(Symbols are the experimental data points)
"Theoretical" Nernst equation predictions
"Empirical" Nernst equation and best straight line predictions
SOLUTION REDOX POTENTIAL - mV vs. S.H.E.
900
850
800
750
700
650
600
-5
-4
-3
-2
-1
0
1
2
3
4
5
Ln (TOTAL FERROUS/FERRIC CONCENTRATION RATIO)

Fig. 5.4

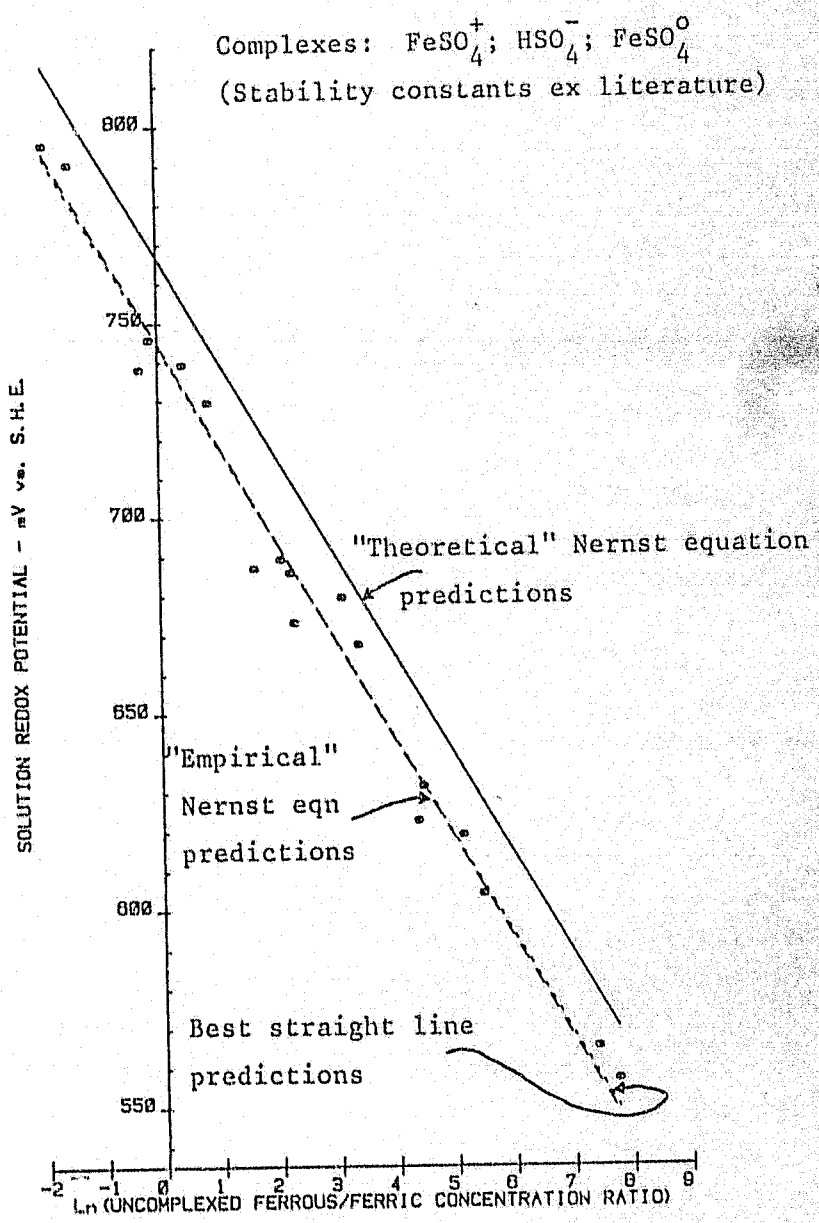

Complexes: $FeSO_4^+$; HSO_4^-; $FeSO_4^o$
(Stability constants ex literature)
"Theoretical" Nernst equation predictions
"Empirical" Nernst eqn predictions
Best straight line predictions
SOLUTION REDOX POTENTIAL - mV vs. S.H.E.
800
750
700
650
600
550
-2
-1
0
1
2
3
4
5
6
7
8
9
Ln (UNCOMPLEXED FERROUS/FERRIC CONCENTRATION RATIO)

Fig. 5.5

Author Dry M J
Name of thesis Kinetics of leaching of a low grade matte in ferric sulphate solution 1984

PUBLISHER:
University of the Witwatersrand, Johannesburg
©2013

LEGAL NOTICES:

Copyright Notice: All materials on the University of the Witwatersrand, Johannesburg Library website are protected by South African copyright law and may not be distributed, transmitted, displayed, or otherwise published in any format, without the prior written permission of the copyright owner.

Disclaimer and Terms of Use: Provided that you maintain all copyright and other notices contained therein, you may download material (one machine readable copy and one print copy per page) for your personal and/or educational non-commercial use only.

The University of the Witwatersrand, Johannesburg, is not responsible for any errors or omissions and excludes any and all liability for any errors in or omissions from the information on the Library website.